Calhoun
Institutional Archive of the Naval Postgraduate School

Calhoun: The NPS Institutional Archive
DSpace Repository

Theses and Dissertations 1. Thesis and Dissertation Collection, all items

1976

An experimental investigation of the whistler nozzle and an analytical investigation of a ring wing in supersonic flow.

Weiss, Donald L.

Monterey, California. Naval Postgraduate School

http://hdl.handle.net/10945/17771

Downloaded from NPS Archive: Calhoun

DUDLEY
KNOX
LIBRARY

Calhoun is the Naval Postgraduate School's public access digital repository for research materials and institutional publications created by the NPS community. Calhoun is named for Professor of Mathematics Guy K. Calhoun, NPS's first appointed -- and published -- scholarly author.

Dudley Knox Library / Naval Postgraduate School
411 Dyer Road / 1 University Circle
Monterey, California USA 93943

http://www.nps.edu/library

AN EXPERIMENTAL INVESTIGATION OF THE WHISTLER NOZZLE AND AN ANALYTICAL INVESTIGATION OF A RING WING IN SUPERSONIC FLOW

Donald L. Weiss

[illegible] SCHOOL
[illegible]

NAVAL POSTGRADUATE SCHOOL
Monterey, California

THESIS

AN EXPERIMENTAL INVESTIGATION OF THE WHISTLER NOZZLE AND AN ANALYTICAL INVESTIGATION OF A RING WING IN SUPERSONIC FLOW

by

Donald L. Weiss
March 1976

Thesis Advisor: M. F. Platzer

Approved for public release; distribution unlimited.

T173040

REPORT DOCUMENTATION PAGE		READ INSTRUCTIONS BEFORE COMPLETING FORM
1. REPORT NUMBER	2. GOVT ACCESSION NO.	3. RECIPIENT'S CATALOG NUMBER
4. TITLE (and Subtitle) AN EXPERIMENTAL INVESTIGATION OF THE WHISTLER NOZZLE AND AN ANALYTICAL INVESTIGATION OF A RING WING IN SUPERSONIC FLOW		5. TYPE OF REPORT & PERIOD COVERED Master's Thesis; March 1976
		6. PERFORMING ORG. REPORT NUMBER
7. AUTHOR(s) Donald L. Weiss		8. CONTRACT OR GRANT NUMBER(s)
9. PERFORMING ORGANIZATION NAME AND ADDRESS Naval Postgraduate School Monterey, California 93940		10. PROGRAM ELEMENT, PROJECT, TASK AREA & WORK UNIT NUMBERS
11. CONTROLLING OFFICE NAME AND ADDRESS Naval Postgraduate School Monterey, California 93940		12. REPORT DATE March 1976
		13. NUMBER OF PAGES 96
14. MONITORING AGENCY NAME & ADDRESS(if different from Controlling Office) Naval Postgraduate School Monterey, California 93940		15. SECURITY CLASS. (of this report) Unclassified
		15a. DECLASSIFICATION/DOWNGRADING SCHEDULE

16. DISTRIBUTION STATEMENT (of this Report)

Approved for public release; distribution unlimited.

17. DISTRIBUTION STATEMENT (of the abstract entered in Block 20, if different from Report)

18. SUPPLEMENTARY NOTES

19. KEY WORDS (Continue on reverse side if necessary and identify by block number)

Ring Wing, Whistler Nozzle, Entrainment, Thrust Augmentation

20. ABSTRACT (Continue on reverse side if necessary and identify by block number)

This thesis consists of two parts. First, an experimental investigation of a new device called the whistler nozzle was conducted. Experiments were conducted in the areas of nozzle efficiency, mass entrainment, and flow visualization. Flow visualization showed the presence of a Coanda type jet wall interaction in the nozzle collar. Thrust efficiencies indicated that whistling could be achieved without much greater losses

20.

than the basic axisymmetric jet. Entrainment tests were inconclusive regarding the whistler nozzle performance. Second, supersonic flow past an oscillating cylindrical shell is analyzed using linearized characteristics methods. Pressure distributions and generalized aerodynamic forces are calculated and presented for various radius to length ratios and reduced frequencies. Good agreement is obtained in the two dimensional limiting case with previous work by Platzer, and an early solution of the steady cylindrical case by Zierep.

AN EXPERIMENTAL INVESTIGATION OF THE WHISTLER NOZZLE AND AN ANALYTICAL INVESTIGATION OF A RING WING IN SUPERSONIC FLOW

by

Donald L. Weiss
Second Lieutenant, USMC
B.S.A.E., USNA, 1974

Submitted in partial fulfillment of the
requirements for the degree of

MASTER OF SCIENCE IN AERONAUTICAL ENGINEERING

from the
NAVAL POSTGRADUATE SCHOOL
March 1976

DUDLEY KNOX LIBRARY
NAVAL POSTGRADUATE SCHOOL
MONTEREY CALIFORNIA 93940

ABSTRACT

This thesis consists of two parts. First, an experimental investigation of a new device called the whistler nozzle was conducted. Experiments were conducted in the areas of nozzle efficiency, mass entrainment, and flow visualization. Flow visualization showed the presence of a Coanda type jet wall interaction in the nozzle collar. Thrust efficiencies indicated that whistling could be achieved without much greater losses than the basic axisymmetric jet. Entrainment tests were inconclusive regarding the whistler nozzle performance. Second, supersonic flow past an oscillating cylindrical shell is analyzed using linearized characteristics methods. Pressure distributions and generalized aerodynamic forces are calculated and presented for various radius to length ratios and reduced frequencies. Good agreement is obtained in the two-dimensional limiting case with previous work by Platzer, and an early solution of the steady cylindrical case by Zierep.

TABLE OF CONTENTS

LIST OF FIGURES.. 6

ACKNOWLEDGEMENT.. 8

I. INTRODUCTION-THE WHISTLER NOZZLE................. 9

II. RELATED PAST WORK................................ 12

III. SCOPE OF RESEARCH................................ 18

IV. NOZZLE DESCRIPTION............................... 19

V. DESCRIPTION OF EXPERIMENTS....................... 21

  A. THRUST EFFICIENCIES......................... 21

  B. MASS ENTRAINMENT............................ 24

  C. FLOW VISUALIZATION.......................... 32

VI. RESULTS AND DISCUSSION........................... 36

VII. CONCLUSIONS AND RECOMMENDATIONS.................. 45

VIII. INTRODUCTION- THE RING WING....................... 46

IX. PROBLEM FORMULATION.............................. 47

X. METHOD OF CHARACTERISTICS........................ 52

XI. GENERALIZED AERODYNAMIC FORCE.................... 55

XII. RESULTS AND DISCUSSION........................... 57

XIII. CONCLUSIONS AND RECOMMENDATIONS.................. 66

APPENDIX A ISENTROPIC THRUST CALCULATIONS............... 67

APPENDIX B ENTRAINMENT RATIO CALCULATIONS............... 68

APPENDIX C ENTRAINMENT CHAMBER DESIGN................... 70

APPENDIX D PROGRAM LISTINGS AND DOCUMENTATION........... 74

LIST OF REFERENCES...................................... 94

INITIAL DISTRIBUTION LIST............................... 96

LIST OF FIGURES

1. Whistler Nozzle Cross Section........................ 11
2. Various Whistler Configurations........................ 13
3. Coanda Effect.................................... 16
4. Whistler Nozzle and Plenum........................ 20
5. Thrust Bed.. 22
6. Thrust Bed Calibration Curve........................ 23
7. Experimental Thrust Curve........................ 25
8. Entrainment Chamber Cutaway View.................... 28
9. The entrainment Chamber and Peripheral Gear......... 29
10. Orifice Pressure Difference vs Entrainment Ratio.... 31
11. Tuft Ring Photo.................................. 34
12. Lampblack Pooling Illustration..................... 35
13. Thrust Efficiency Results.......................... 38
14. Entrainment Ratio Results and Comparison Data....... 39
15. Entrainment Ratio vs Reynolds Number............... 40
16. Tuft Pictures, Results.............................. 43
17. Ring Wing Illustration.............................. 48
18. Axial Pressure Distribution, 2D Limiting Case....... 58
19. Axial Pressure Distribution, Comparison With Zierep. 59
20. Numerical Instability Illustration................. 61

21. Pitching Moment vs Reduced Frequency................ 63

22. Pitching Moment vs Outer Radius To Length Ratio..... 64

23. Representative Axial Pressure Distribution, Including One Reflection.................................... 65

ACKNOWLEDGEMENT

I wish to express my great appreciation to Mr. Stan Johnson for his invaluable help and advice throughout the course of this thesis project. I would also like to thank Mr. Ron Ramaker for the excellent work he did in constructing the entrainment chamber, a primary part of this work. Finally, I would like to thank Professor M. F. Platzer whose advice and direction were a great help, and Connie, my wife, without whose help this thesis might never have been written and typed.

I. INTRODUCTION-THE WHISTLER NOZZLE

The phenomenon of entrainment is a process through which a moving fluid increases its mass flow, by "grabbing up" the medium it is flowing in. The moving fluid is called the working fluid, and might be the primary water jet in an ejector pump. The medium might be any other fluid, say oil, in the case of the ejector pump.

The entrainment process has found practical use for quite a long time. Analytical descriptions of the entrainment process exist; however, none is general enough to describe all cases of practical interest. Even the relatively simple case of a steady jet in still air is rather difficult because of the many configurations which one would like to describe. Thus interest and research in this area continues, perhaps with more intensity than previously due to the recent interest in new V/STOL configurations which would employ this process. One such is the Navy's XFV - 12A, which is expected to derive a large amount of thrust through the augmentation, or entrainment, of its primary thrust using wing mounted ejectors.

The success of concepts such as the augmenter wing depends on many factors, an important one being the rate of entrainment of the primary jet, and another being its efficiency. This rate of entrainment is the rate of increase of jet mass flow with axial distance away from the jet nozzle. The rate of entrainment and nozzle efficiency are characteristics which vary with nozzle configuration.

As mentioned earlier , there is a large variety of steady nozzle configurations. Lobe, slot, and hypermixing

nozzles are some which have drawn recent interest for their entrainment capabilities. One should not neglect unsteady nozzle configurations, however, as such effects as swirling the primary flow, and oscillating the primary flow in a bistable manner (fluidic oscillator), also show promise in their ability to entrain.

One of the newest nozzle configurations to surface is an unsteady nozzle. Perhaps the simplest in construction of all unsteady nozzles, it is illustrated in figure 1. The whistler nozzle, as it is called, produces a loud pure tone while in operation. Additionally, it creates a relatively large rate of entrainment. It is the whistler nozzle which is the subject of this thesis.

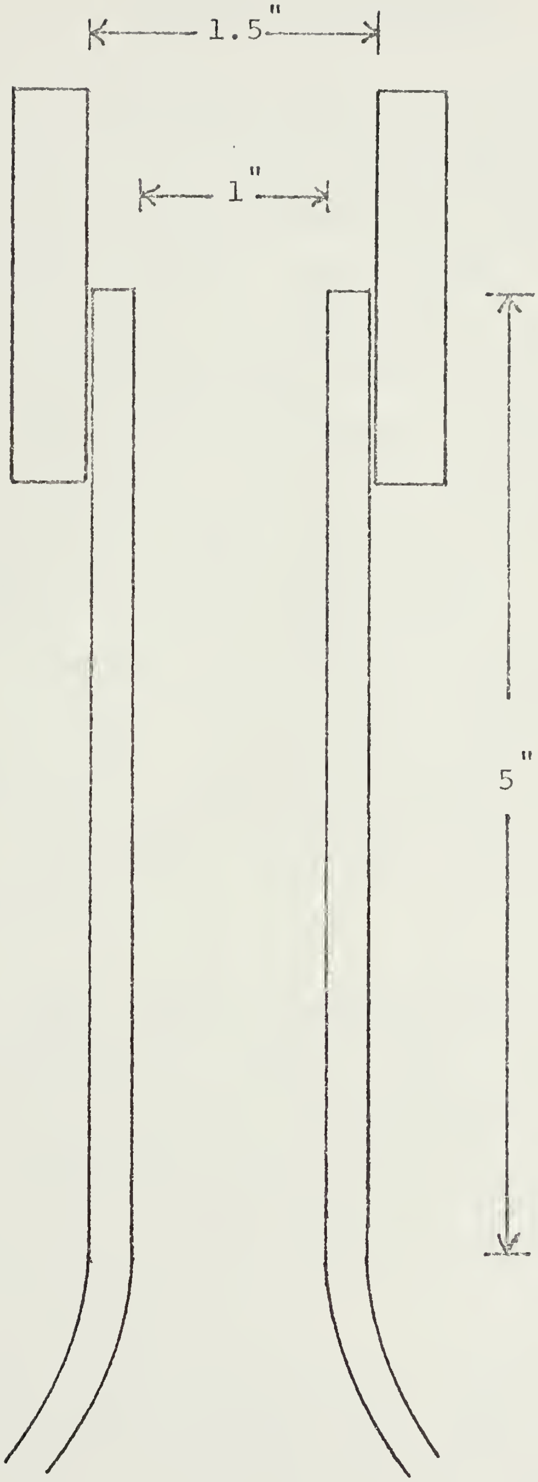

Figure 1 - WHISTLER NOZZLE CROSS SECTION

II. RELATED PAST WORK

The earliest work done on the whistler nozzle was by Hill and Greene (reference 1). In 1974, they cited the discovery of a new phenomenon, characteristic of a new device which they named the whistler nozzle. Their basic configuration, as illustrated in figure 1, consisted of a convergent section, followed by a section of constant area followed by a step change in cross sectional area to another section of constant area. The length of the last section could be varied to produce loud pure tones of varying frequency, through the excitation of a standing acoustic wave in the final section, much as in an organ pipe. Hill and Greene observed that the whistler produced a greatly increased mixing rate, and decided that this was due to acoustic stimulation of the jet. Increased mixing rate of an axisymmetric jet due to acoustic stimulation is a process that had been observed earlier by Crow and Champagne(reference 5).

In addition to the basic axisymmetric configuration, many other configurations were found to produce the whistling phenomenon. A few are illustrated in figure 2. Common to all of these was that the step in cross section had to extend completely around the jet. Also noted was the apparent presence of a separation reattachment cycle, occurring at the nozzle lip.

No further study seems to have been performed concerning the whistler nozzle, save a report in 1975 by Hill and Jenkins (reference 2), in which they reestablished the operating characteristics of the nozzle, and its ability to entrain more air.

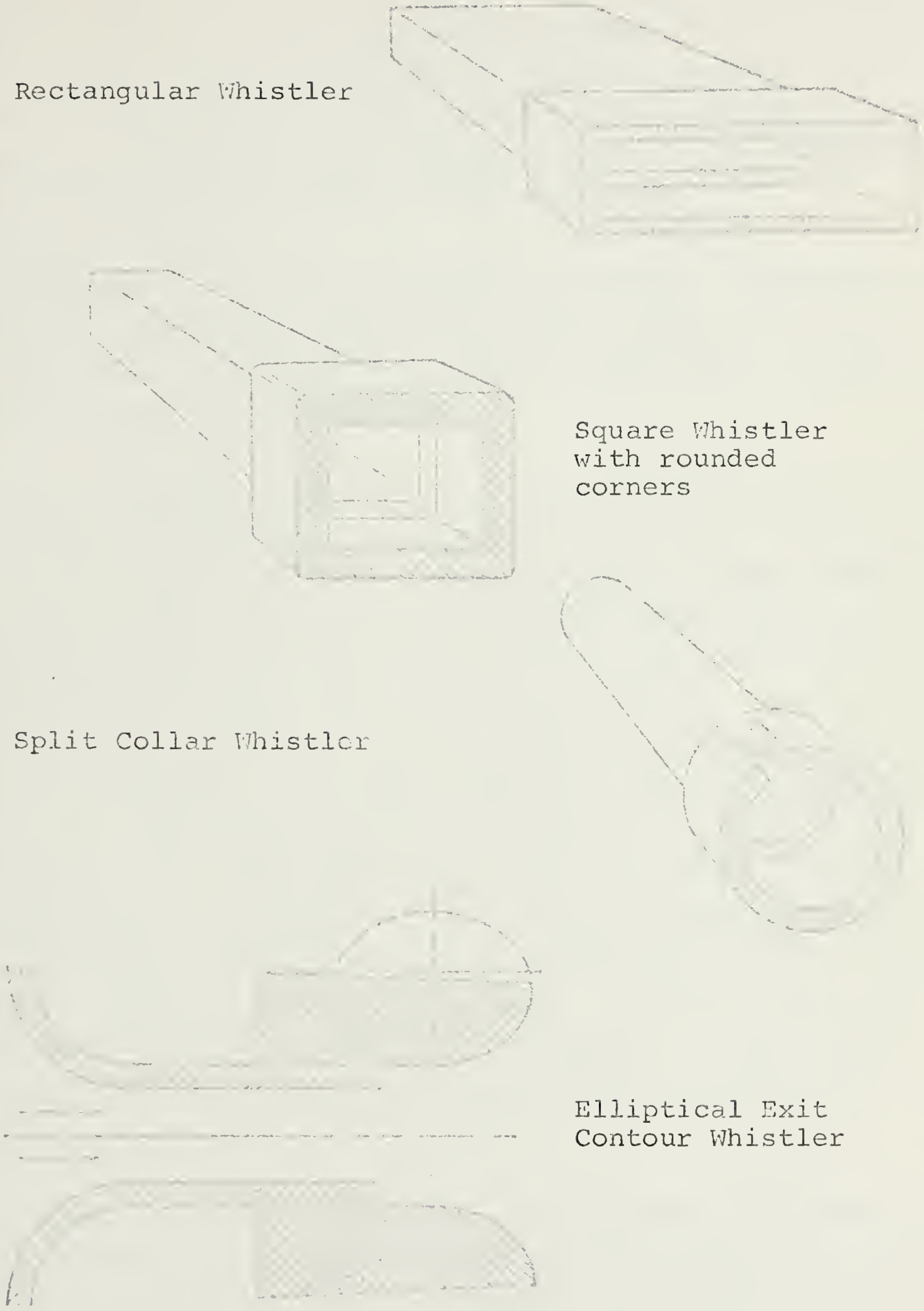

Rectangular Whistler

Square Whistler with rounded corners

Split Collar Whistler

Elliptical Exit Contour Whistler

Figure 2 - VARIOUS WHISTLER CONFIGURATIONS

Hill and Greene's work has been summarized, since their original report, in comprehensive reviews of the ejector state of the art by Schum (reference 3), and by Viets (reference 4). These reports call attention to the whistler nozzle's promise in rate of entrainment, and the lack of data regarding the whistler thrust efficiency.

Although no further research directly involving the whistler is available, much work has been done in the area of free jets, and entrainment, which might prove valuable in a study of the whistler nozzle.

An obviously important area of related work is the sensitivity of free jets to acoustic stimulation. Probably the best known and most definitive work in this area was performed by Crow and Champagne (reference 5). By mounting a speaker inside the plenum chamber they managed to excite a free axisymmetric jet, at various frequencies. The effect of the sound was to produce a velocity fluctuation in the nozzle exit plane. It was observed that the turbulent structure of the jet was sensitive to the acoustic excitation. Through the use of high-speed schlieren photography it was observed that under acoustic stimulation the turbulent structure of the jet developed a large-scale vortex structure, as contrasted with the small scale vortex sheet surrounding a normal jet. Attendant to the formation of the large-scale vortices, an increase in the mixing rate was also observed.

Others, such as Bevilaqua and Lykoudis (reference 6), have observed the turbulent structure in steady, free jets. The presence of a large-scale vortex structure has been observed in such jets at low Reynolds numbers. It appears that the large-scale structure dissappears as Reynolds number increases. However, according to the findings of

Crow and Champagne, it may be reexcited through accustic stimulation. It may be conjectured from experimental evidence that the entrainment process is a combination of a large-scale "scooping up" of the ambient fluid, and a small-scale nibbling away at the ambient fluid. These entrainment processes would correspond to the large and small scale vortex structures around a free jet.

A further area of related research, perhaps not obvious, is the well known Coanda effect. The basic whistler configuration sets up a flow situation somewhat akin to that of a bistable fluidic element, or fluidic oscillator. The difference between the two cases is that the fluidic oscillator oscillates between two positions, while the whistler must oscillate between many circumferential positions. That such an oscillation takes place seems indicated by the nozzle configuration and the separation reattachment cycle noted by Hill and Greene.

Reference 10 provides a good summary of the mechanism of the Coanda effect, as well as its characteristics regarding reattachment and sensitivity to sound. Though the following comments relate specifically to two- dimensional flows, it is thought that the general behavior and mechanism should carry over to a three- dimensional situation.

Figure 3 illustrates the Coanda mechanism in two-dimensional flow. As shown, a jet is issuing from an orifice and flowing between two adjacent walls. Because the jet will at some time be nearer to one wall than the other, and because the jet is entraining air, a pressure difference across the jet will develop that pulls the jet to the closer wall. This attachment forms a region of circulating flow. The point of jet attachment is determined by this region, in which a balance is struck between flow entrained by the jet and flow reinjected by the jet.

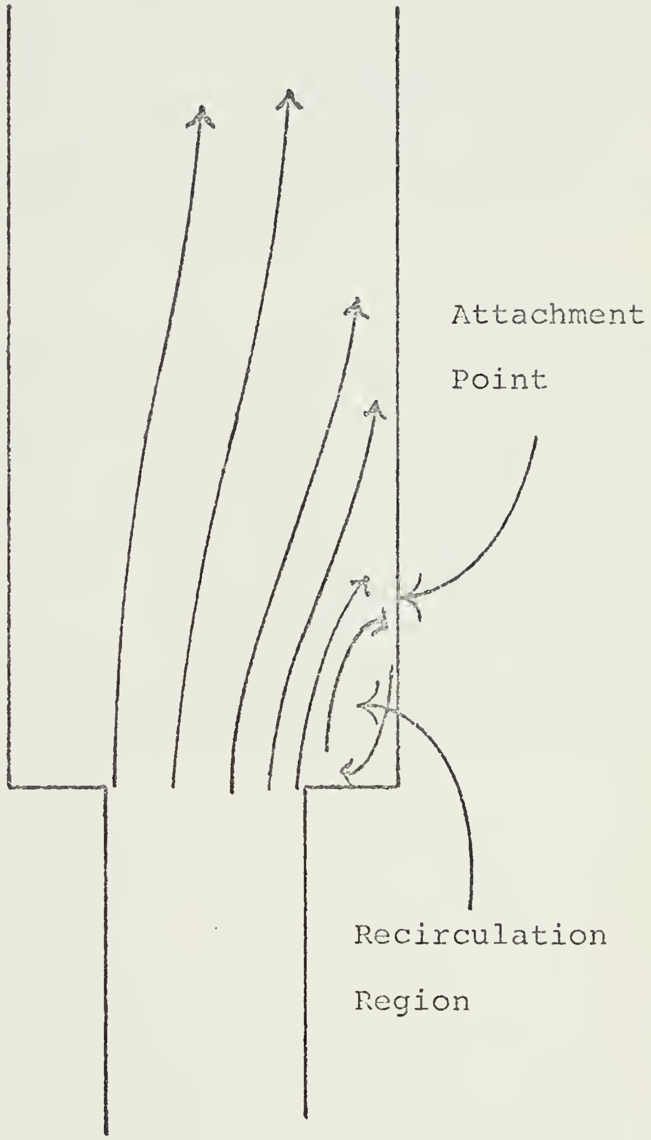

Figure 3 - COANDA EFFECT

Anything that disrupts this balance causes the attachment point of the jet to shift.

Observation has shown that the attachment point in Coanda effect is sensitive to jet velocity and sound, within a range of Reynolds numbers. In the range of Reynolds number from 200 to 3000, under the effect of increasing jet velocity, or a sound input of increasing amplitude, the attachment point has been observed to move upstream. This upstream movement appears to approach a limiting position, beyond which the point will not move.

Reference 10 relates the effects of jet velocity and sound on the attachment point to the point of transition from laminar to turbulent flow of the jet. Both increasing jet velocity and a sound input will move the transition point closer to the jet exit. This movement will increase the length of turbulent flow across the recirculation region. A turbulent jet entrains more air than a laminar jet, and thus the balance of flow in the recirculation region is disrupted, with a resulting upstream move of the attachment point.

III. SCOPE OF RESEARCH

The intent of this research was to provide a clearer insight into the workings of the whistler nozzle, and to develop an improved understanding of the ways in which one may effect control over the characteristics of a free jet.

Specific areas of research were the nozzle thrust efficiency, the nozzle entrainment rate, and visualization of the lip interaction process described by Hill and Greene. Accordingly, experiments were conducted to obtain relevant data. Thrusts were measured on a thrust bed, mass entrainment measured in a device patterned after that developed by Ricou and Spalding (reference 7), and high speed motion pictures taken of tufts about the nozzle lip.

IV. NOZZLE DESCRIPTION

The whistler nozzle used in all tests is illustrated in figure 4. It consisted of a small plenum, convergent section, short constant area section and a moveable collar over the constant area section. The inner whistler diameter was 1 inch, while the collar diameter was 1.5 inches. The nozzle configuration was essentially that used by Hill and Greene in their investigations. The characteristic dimension used for Reynolds number and nondimensionalization of axial distance from the nozzle was the inner nozzle diameter, 1 inch.

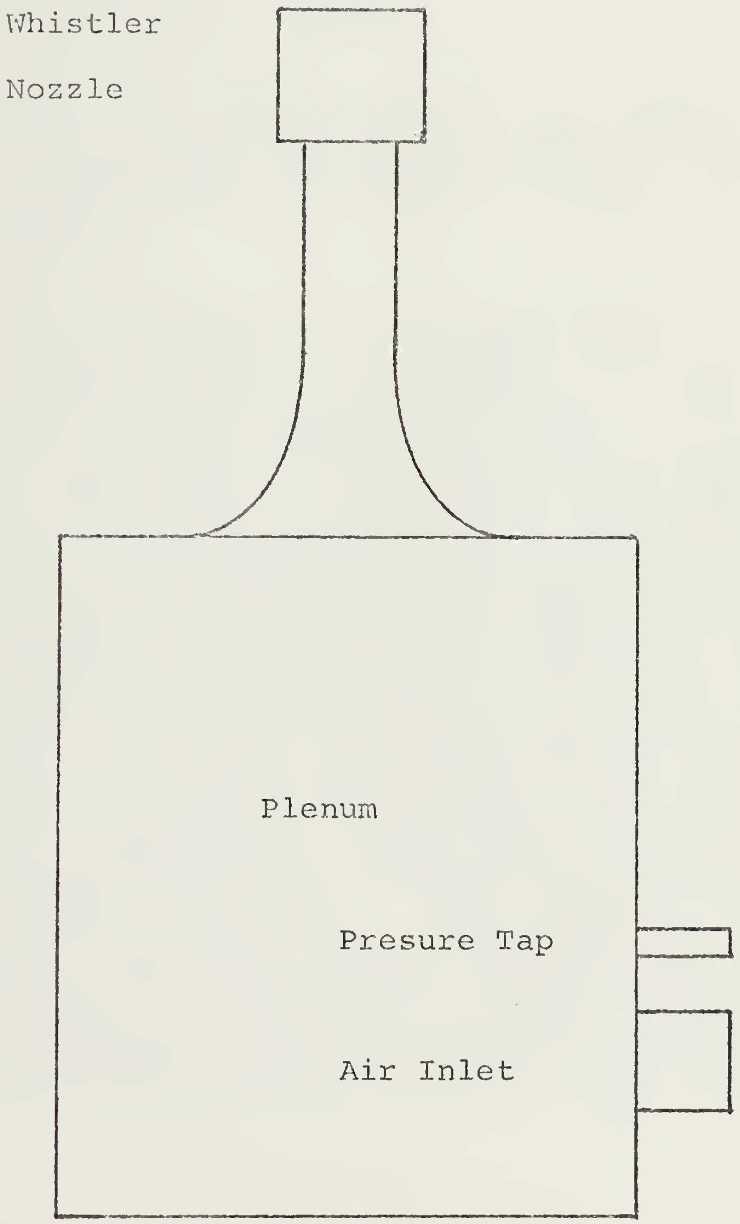

Figure 4 - WHISTLER NOZZLE AND PLENUM

V. DESCRIPTION OF EXPERIMENTS

A. THRUST EFFICIENCIES

Thrust efficiencies were obtained by measuring nozzle thrust. A comparison was made between measured and calculated thrust.

Test equipment consisted of a thrust bed and the nozzle. The thrust bed was configured to measure horizontal thrust, and slid on two tracks, mounted to a solid foundation. The nozzle plenum was clamped to the thrust bed which was in turn secured to the foundation through a load ring, mounted with a load cell, the device that actually measured thrust. Air was supplied to the nozzle from a large tank, connected to the plenum through a regulator and a flexible tube which led vertically away from the plenum, so as not to bias the thrust measurements in any way. Calibration was performed with the use of a tray, connected to the bed through a cable and pulley arrangement, upon which one placed weights of known magnitude. Peripheral gear required included a voltage source, digital voltage meter, and Wheatstone bridge. Figure 5 illustrates the set up. Plenum pressures were measured using a mercury manometer.

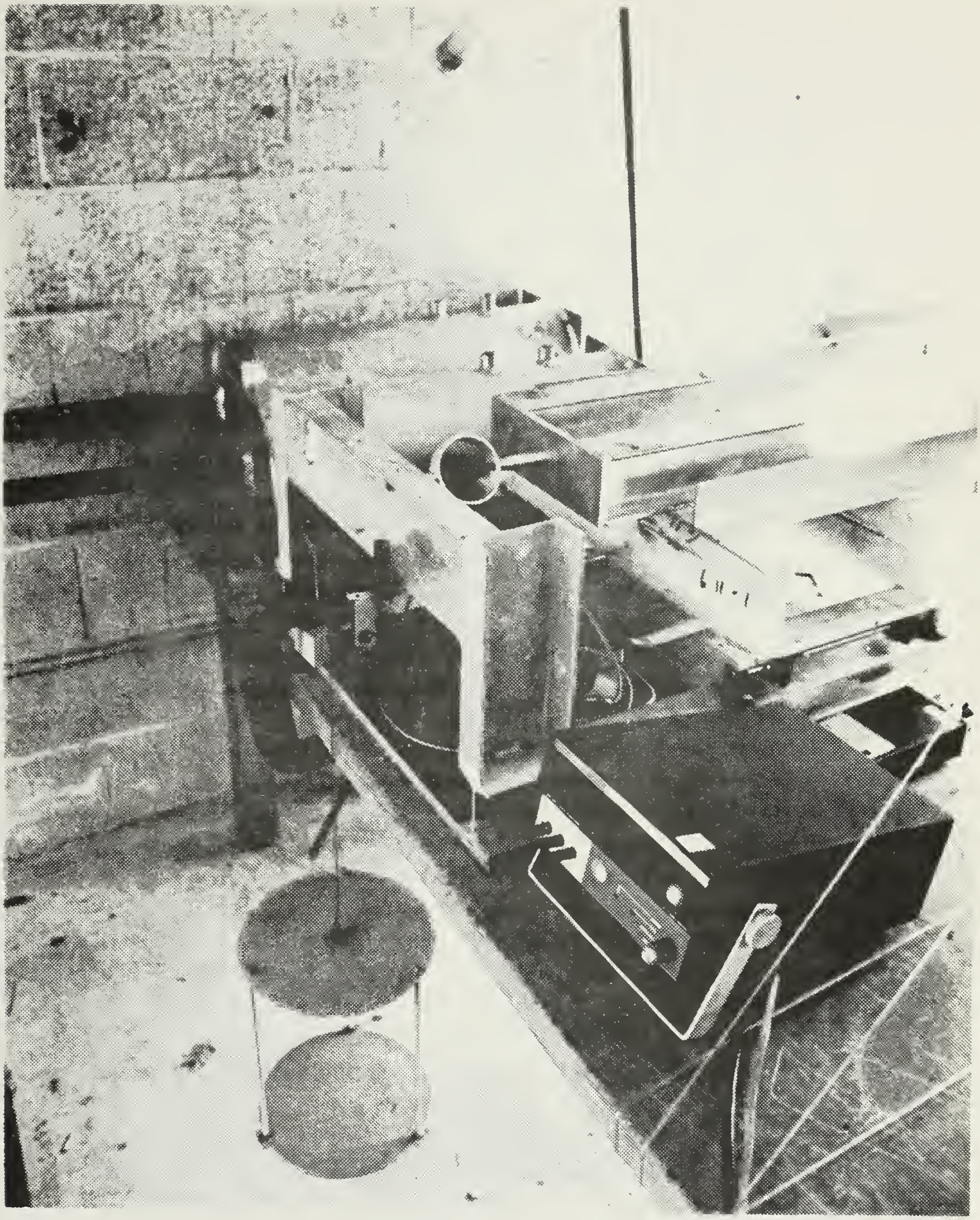

Figure 5 - THRUST BED

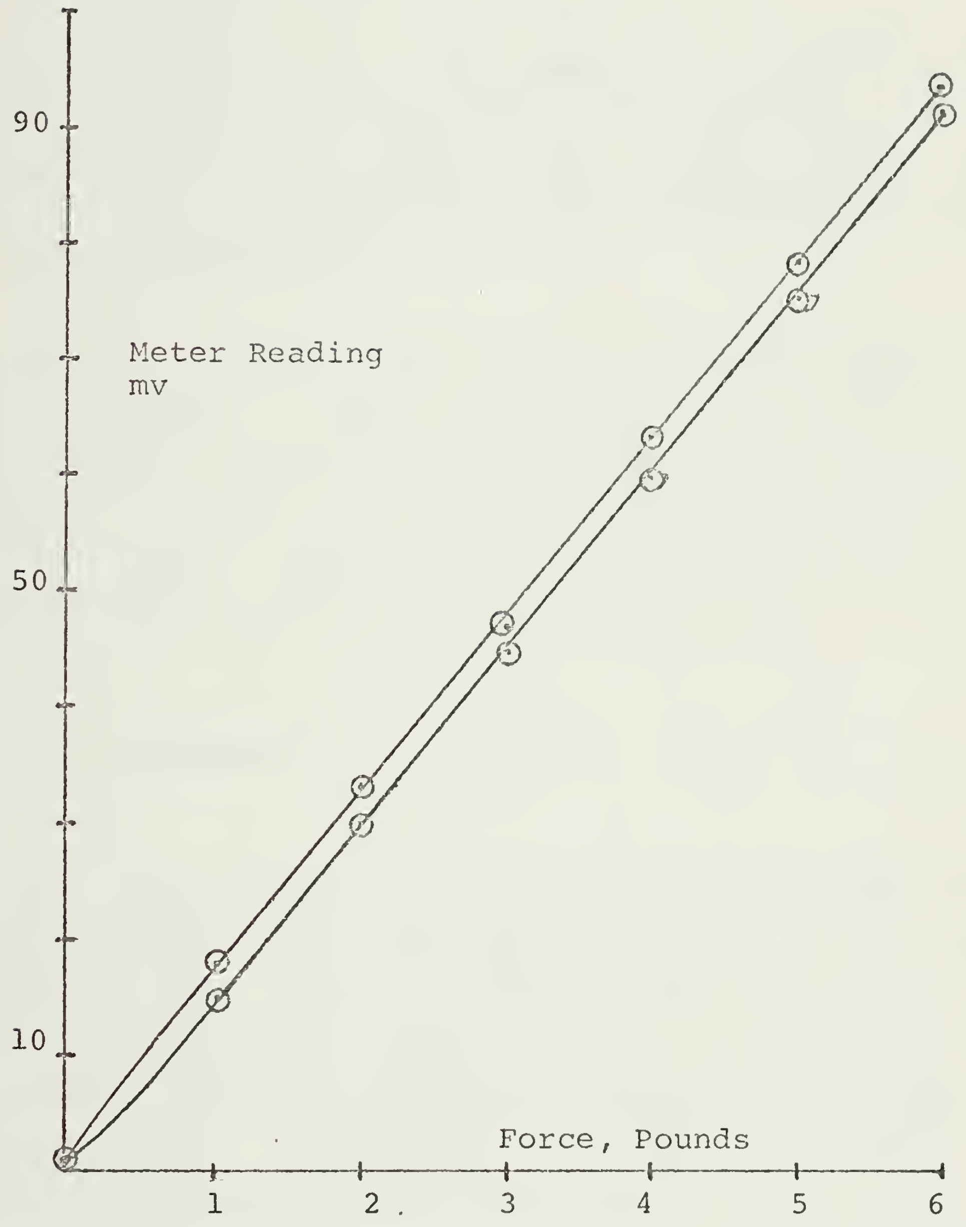

Figure 6 - THRUST BED CALIBRATION CURVE

Calibration of the thrust bed indicated a certain amount of hysteresis in the system, as may be seen in figure 6. Not serious at thrusts of about 6 pounds, it did introduce problems at low thrust levels, and precluded reliable thrust measurement at low Reynolds numbers.

Thrust measurements were made for various collar positions, over a range of nozzle exit velocities. Recorded data included gage pressure in the nozzle plenum, thrust readings from the voltmeter, collar extension, and ambient pressure and temperature.

Measured thrusts were plotted against pressure ratio across the nozzle. Figure 7 presents an example curve. Ideal thrust was calculated according to the procedures in appendix A. Thrust efficiencies were then obtained and plotted against nozzle pressure ratio, exit velocity, and Reynolds number (based on the nozzle diameter).

B. MASS ENTRAINMENT

Mass entrainment was measured directly, using a device patterned after one developed by Ricou and Spalding (reference 7). It was believed that this device should yield more accurate results than an approach using integrated velocity profiles, especially in the case of an unsteady nozzle. Measurements were made at various axial positions, for several collar positions.

The device used will hereafter be referred to as the entrainment chamber. It was designed with the aid of data from a research report by Peschke (reference 8). Appendix B provides a detailed account of the design.

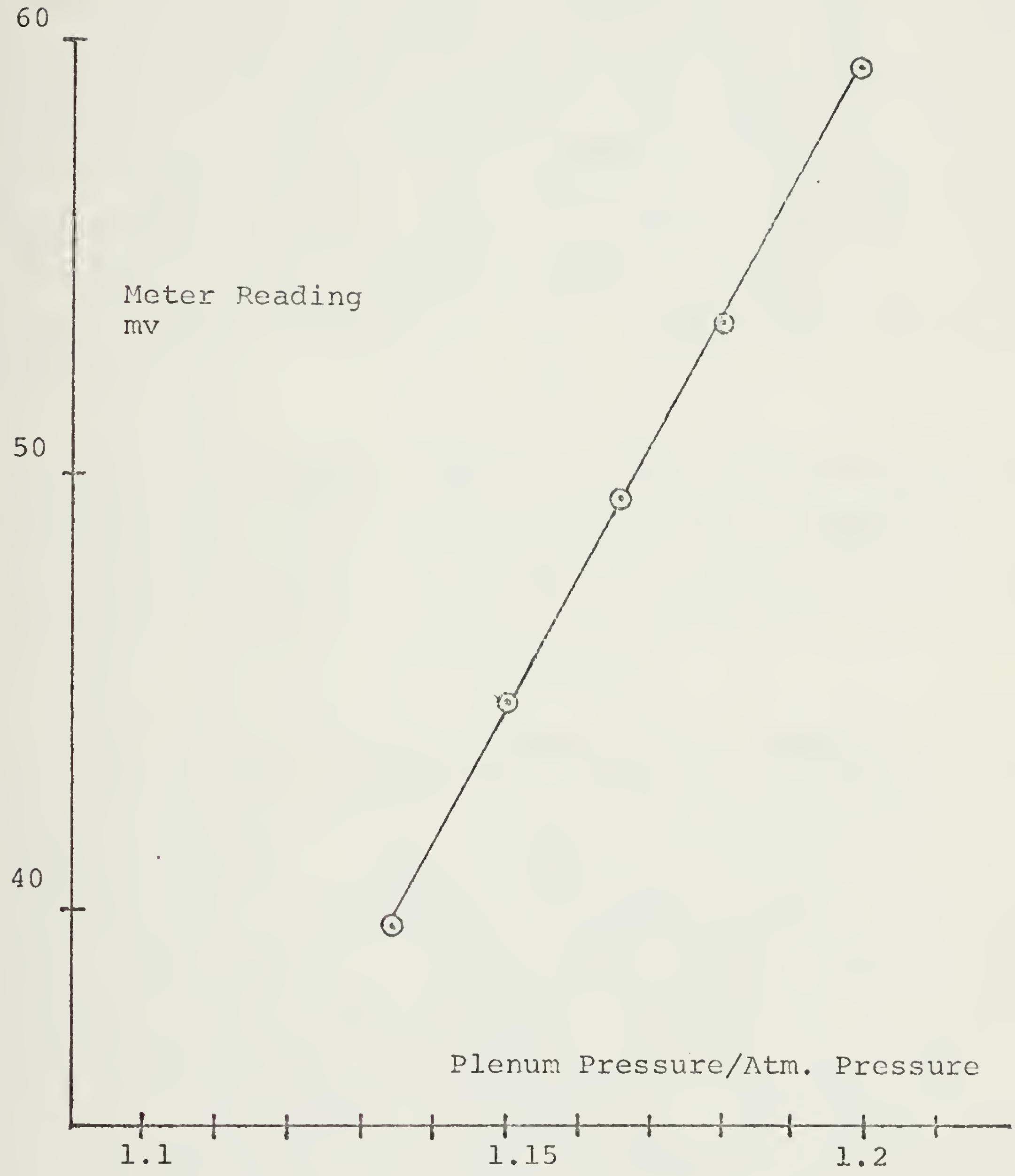

Figure 7 - EXPERIMENTAL THRUST CURVE

The principle of operation is relatively simple. The entrained air of a free jet flows in at a right angle to the jet axis. The entrainment chamber simply blocks this inflow with a circumferential membrane, and seals the ends with a plate at the nozzle and an orifice at the axial station where one wishes to measure the total mass flow. Ideally, all of the entrained air is supplied to the exterior of the membrane from a regulated source. As a free jet does not support any axial pressure gradient, the proper amount of air to supply through the membrane is indicated by the disappearance of any pressure gradient across the orifice. One may regulate the membrane flow to obtain this point. These primary aspects of the device are illustrated in figure 8.

Critical design aspects of the entrainment chamber, especially the orifice sizes, are treated in appendix B. It is sufficient here to simply state that one entrainment chamber was designed to perform measurement of the total jet mass flow at various axial locations.

One primary difference between this chamber's geometry and that of others (references 7 and 8) should be noted. As shown in figure 8, exit orifices were positioned in the porous cylinder at various distances from the nozzle. That portion of the porous cylinder extending above the orifice plate was sealed by a fiberglass cylinder attached to the orifice. Thus,in this situation that portion of the jet beyond the orifice and inside the porous cylinder exit was not in a truly free-jet flow situation. This was as opposed to the reference 7 and 8 configurations where the exit orifice corresponded to the exit of the porous cylinder. Thus, in those experiments the jet past the orifice was in a truly free-jet flow situation. The configuration used in this report was adopted in order to facilitate the measurement of mass flows at many axial locations. It was

hoped that this chamber's geometry would not affect the chamber readings greatly, although some effect was to be expected.

Peripheral equipment to the basic entrainment chamber included flow regulating, metering, and measuring devices. Figure 9 presents a photograph of the chamber and its peripheral gear. Separate air sources, both fed by a large tank, were supplied for the nozzle and membrane. Nozzle flow was metered through an orifice and controlled with a regulator. Because of the much greater mass flow required, membrane air was supplied through a venturi, followed again by a flow regulator. Pressures across the orifice were measured with an inclined water manometer. Pressures across the venturi were measured with a mercury manometer. Pressure across the entrainment chamber orifices was measured with an alchohol micromanometer. Nozzle plenum pressure was measured with a water manometer.

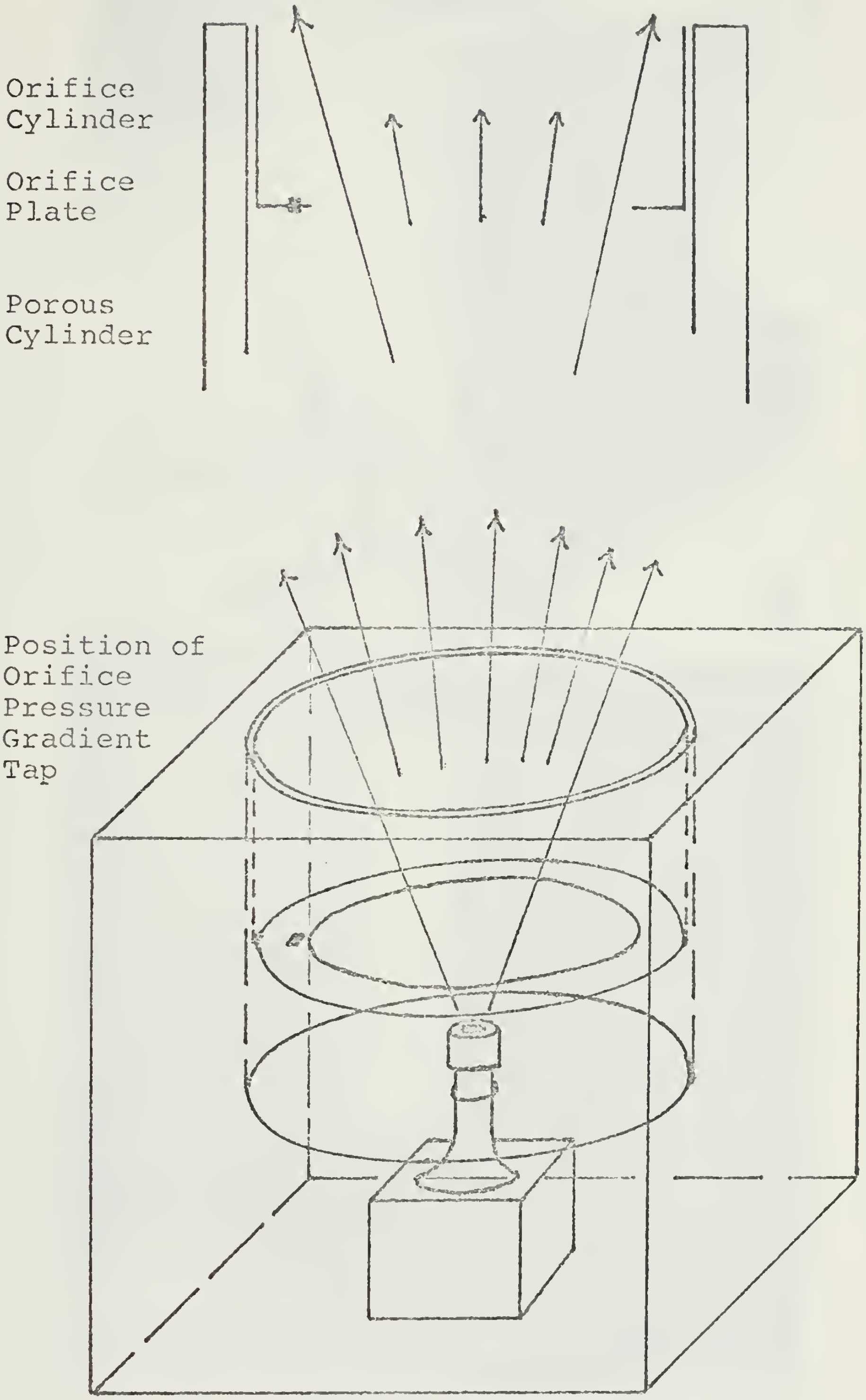

Figure 8 - ENTRAINMENT CHAMBER CUTAWAY VIEW

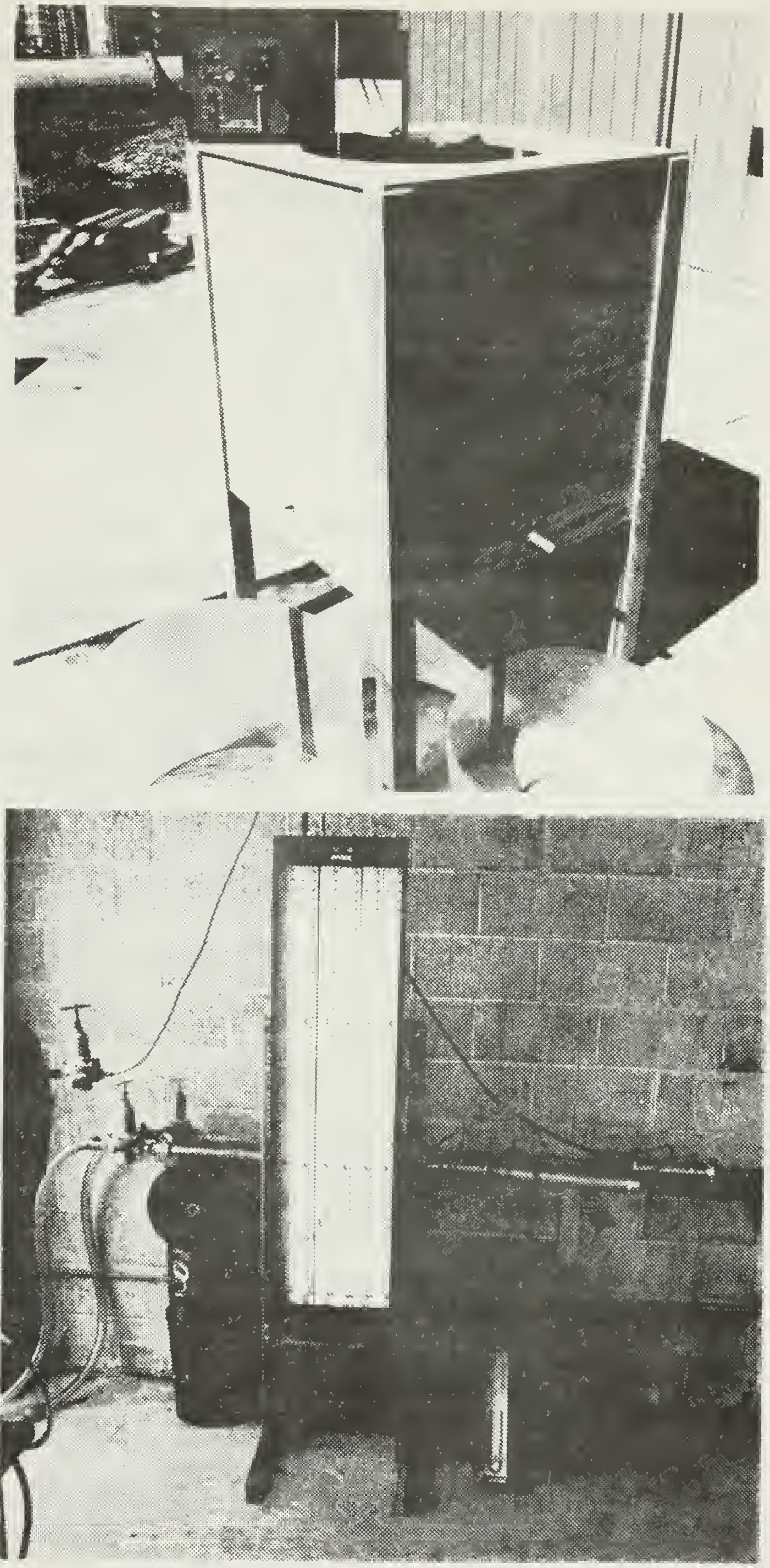

Figure 9 - THE ENTRAINMENT CHAMBER AND PERIPHERAL GEAR

Membrane air temperature was measured just after the venturi, using a mercury thermometer.

Entrainment measurements were made at various axial locations for various collar positions. Recorded data included pressure difference across the venturi and orifice, pressure difference across the entrainment chamber orifice, nozzle plenum pressure, ambient pressure, air temperature in the membrane supply, and collar position. Standard procedure for each run was to vary the membrane airflow so that one obtained both positive and negative pressure gradients at the chamber orifice. This provided a more precise location of the proper entrained flow rate. It is of interest to note that, due to hardware limitations and the large amount of air entrained by the jet at the furthest axial locations measured, nozzle exit velocities were limited to around 100 feet per second at the further axial locations. This also affected the number of useful locations for whistler measurements, as a strong whistler oscillation required a relatively large exit velocity, say 300 feet per second.

Data reduction followed standard procedures for the venturi and orifice. These are presented in appendix C. Entrainment was plotted as M/MO (total mass flow divided by the primary mass flow), against X/D, axial location divided by nozzle diameter. Working curves of chamber orifice pressure gradient are presented as pressure difference against M/MO, in the example plotted in figure 10.

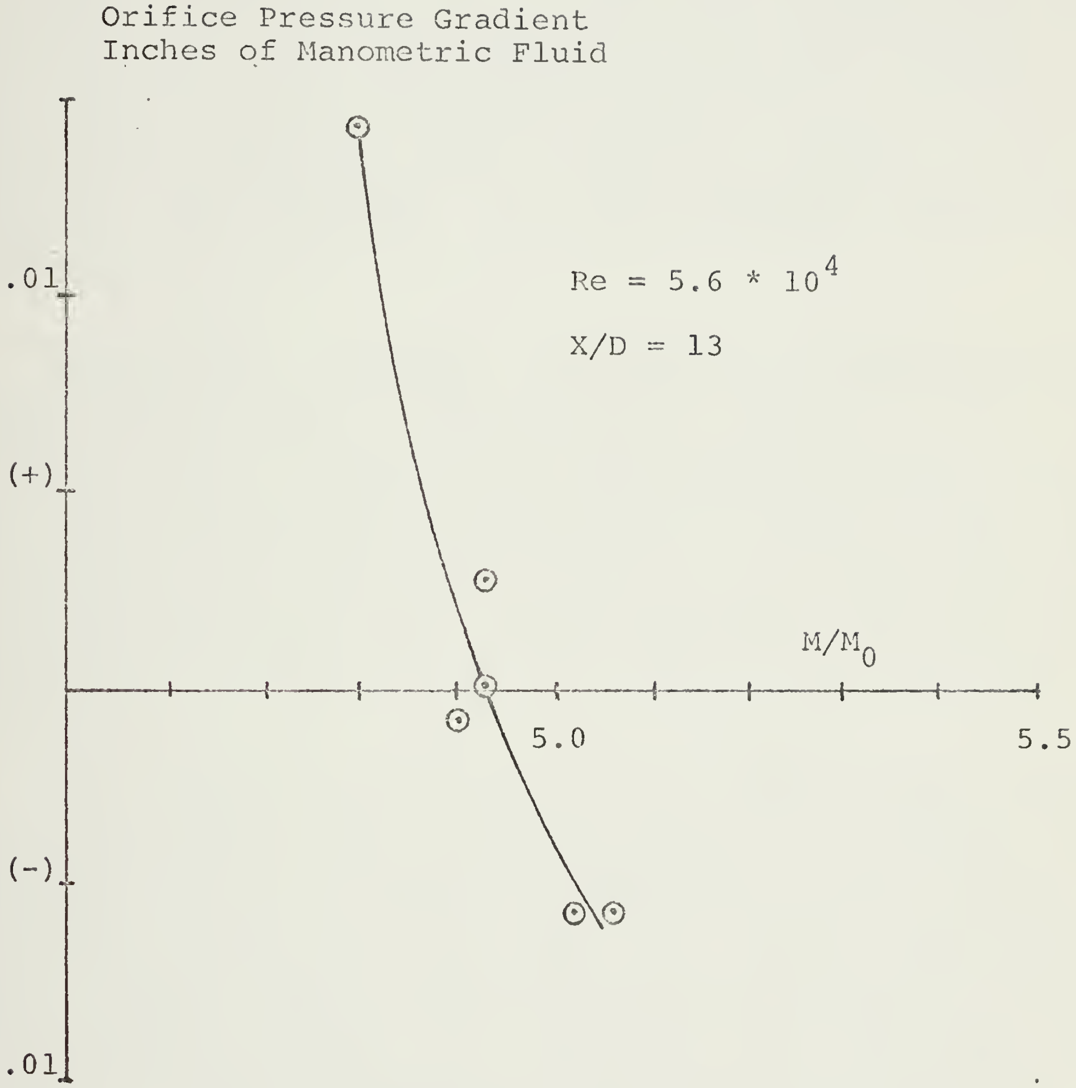

Figure 10 - ORIFICE PRESSURE DIFFERENCE VS ENTRAINMENT RATIO

C. FLOW VISUALIZATION

Flow visualization of the nozzle jet lip interaction was performed in two ways: high-speed motion photography of a ring of tufts at the nozzle lip, for the purpose of discerning a pattern to the interactions; and a mixture of lamp black and kerosene inside the nozzle collar in order to observe the behavior of the separation reattachment location.

Photographic equipment consisted of a Honeywell Pentax single reflex camera, a Bolex Supreme handheld 16mm movie camera, and a Redlake Hycam 16mm high-speed movie camera. The tuft ring was simply constructed of cotton threads held by a masking tape ring, and a photo of the ring is presented in figure 11. Observation in the lampblack experiment was performed with the naked eye and no peripheral equipment was necessary.

Photographic tests were to be done in three phases. High-speed still shots were first taken to determine the usefulness of the tufts for visualization, and to obtain the approximate required film speed for motion photography. Next, medium speed motion pictures, 64 frames per second, were taken to confirm the necessity of the high-speed camera. Finally, high-speed motion pictures were taken to visually control the tuft motion such that useful observations could be made. No particular collar settings or exit velocities were used in photographic work. The only requirement was to produce the oscillation phenomenon, which was never difficult. As it turned out, a lack of time prevented the completion of the high-speed photography phase.

Lampblack tests were performed in two ways. The inside of the collar extension was liberally coated with the lampblack mixture, and either exit velocity varied at constant collar setting, or collar setting varied at constant exit velocity. Observations were all visual, none quantitative, save noting the range of exit velocities covered, which was from about 100 to 300 feet per second. The lampblack mixture was observed to pool as illustrated in figure 12, and the downstream-most edge of the pool was interpreted as indicating the location on the collar of reattachment and separation.

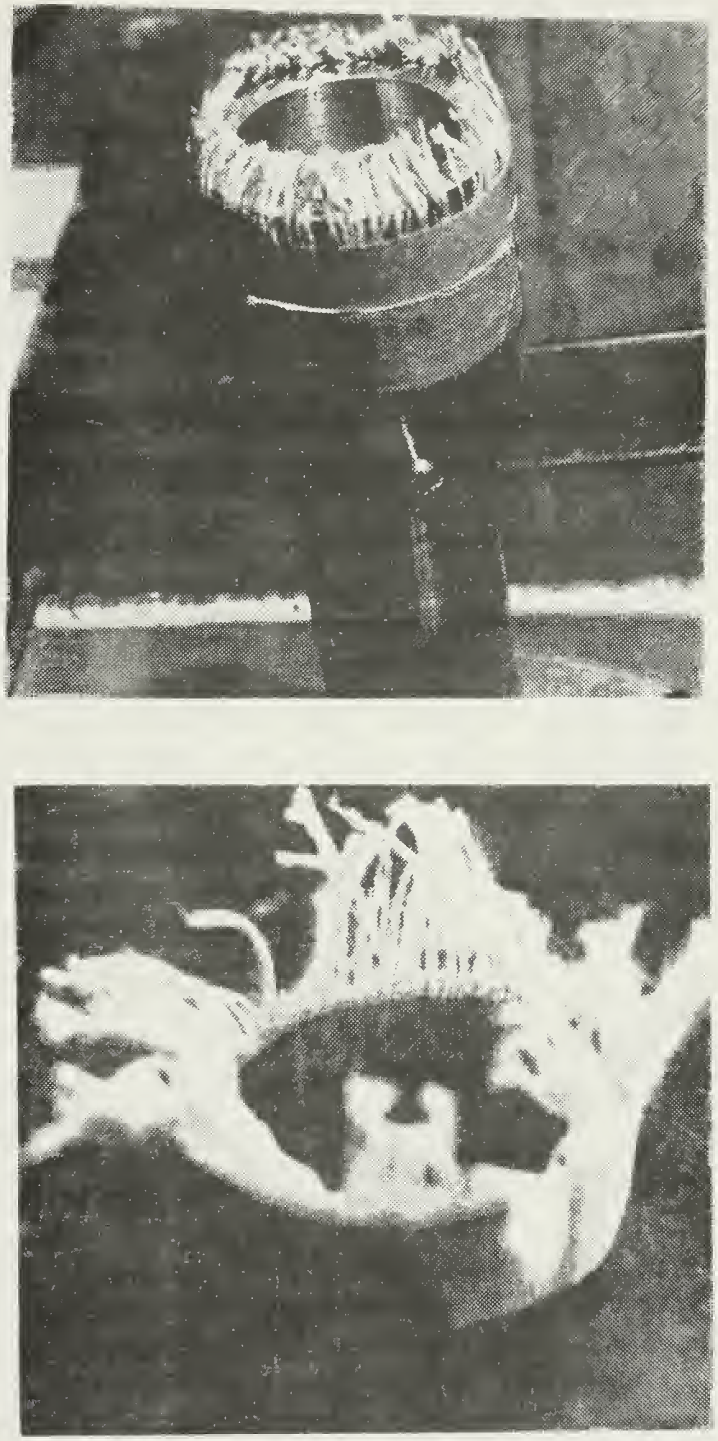

Figure 11 - TUFT RING PHOTO

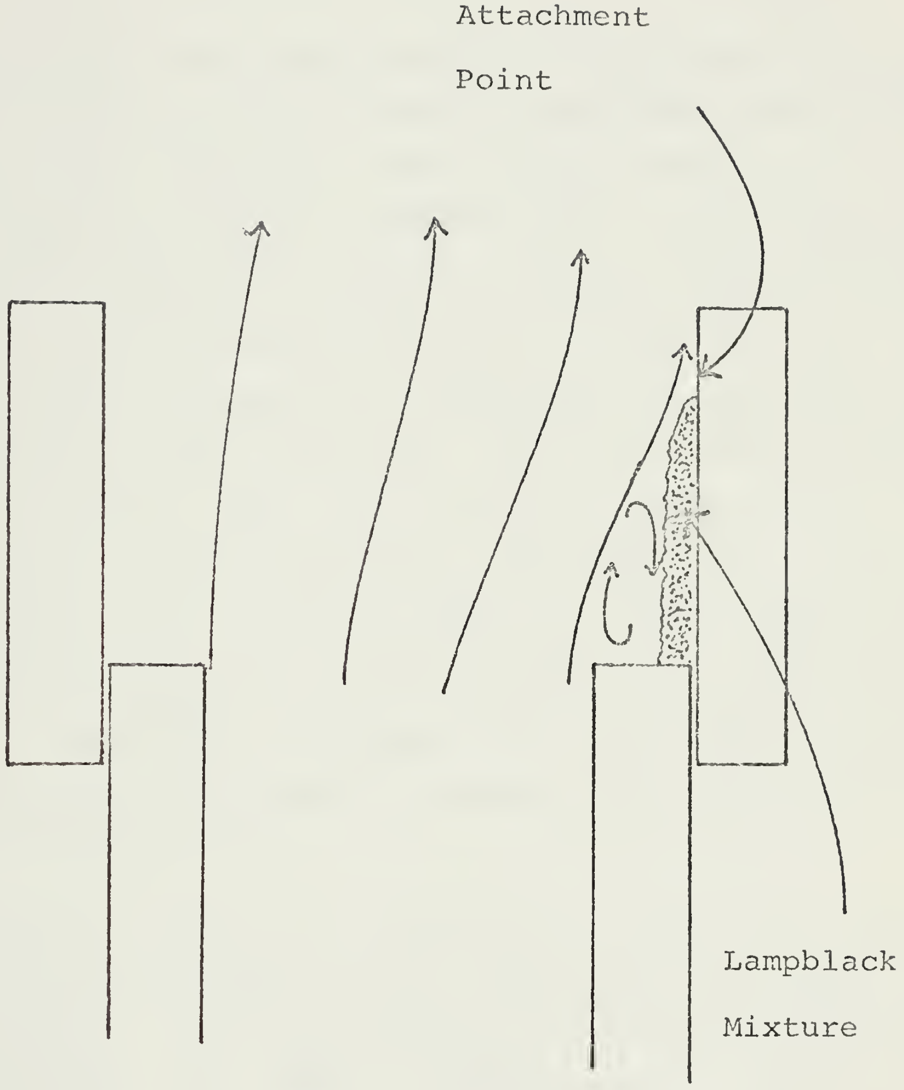

Figure 12 - LAMPBLACK POOLING ILLUSTRATION

VI. RESULTS AND DISCUSSION

Nozzle thrust efficiency results are presented in figure 13, plotted for various collar positions. The whistler oscillation was produced at each collar setting for the whole range of Reynolds numbers shown, although sudden frequency jumps did occur in this range. These frequency jumps did not appear to change the nozzle thrust or thrust efficiency in any discontinuous manner. Instead the trend was as indicated, progressively decreasing nozzle efficiency with increasing collar extension. The zero collar extension efficiencies were found to be about 6 percent lower than those found in a previous report (reference 8). This is believed due to the extremely simple, unflared configuration of the nozzle, which may be seen in figure 4. Reference 8 nozzles were divergent nozzles and as such should be more efficient. Important to note is that the whistler oscillations may be obtained without much reduction in the basic nozzle efficiency.

Entrainment results are presented in figure 14, plotted together with the results of Hill and Greene (reference 1) for comparison. As may be seen, in the case of the basic jet agreement is good qualitatively but poor quantitatively. In the case of the whistler nozzle agreement is not good in any way. It is believed that the poor quantitative comparison was due to interference of the deep orifice cylinders with the jet. These create a pressure gradient from the orifice to the chamber exit which quite possibly affects the readings. As noted in the experiment section, and in Appendix C, these orifice cylinders constitute a major difference in configuration

from the chambers of reference 7 and 8. Additionally, in the case of the whistler nozzle, it is believed the method of enclosing the jet up to the axial position of measurement may interfere with the sound - jet interaction (especially the cloth porous cylinder) and the formation of a large-scale turbulent structure. Figure 15 illustrates that readings taken were relatively constant with Reynolds number. As noted by Ricou and Spalding, the entrainment ratio can be a strong function of Reynolds number in certain ranges of Reynolds number. It is interesting to note that this behavior is supported by the present notion of jet turbulence structure and its development as exit velocity increases, which postulates that the major contributor to entrainment, the large scale structure, dissappears as Reynolds number increases.

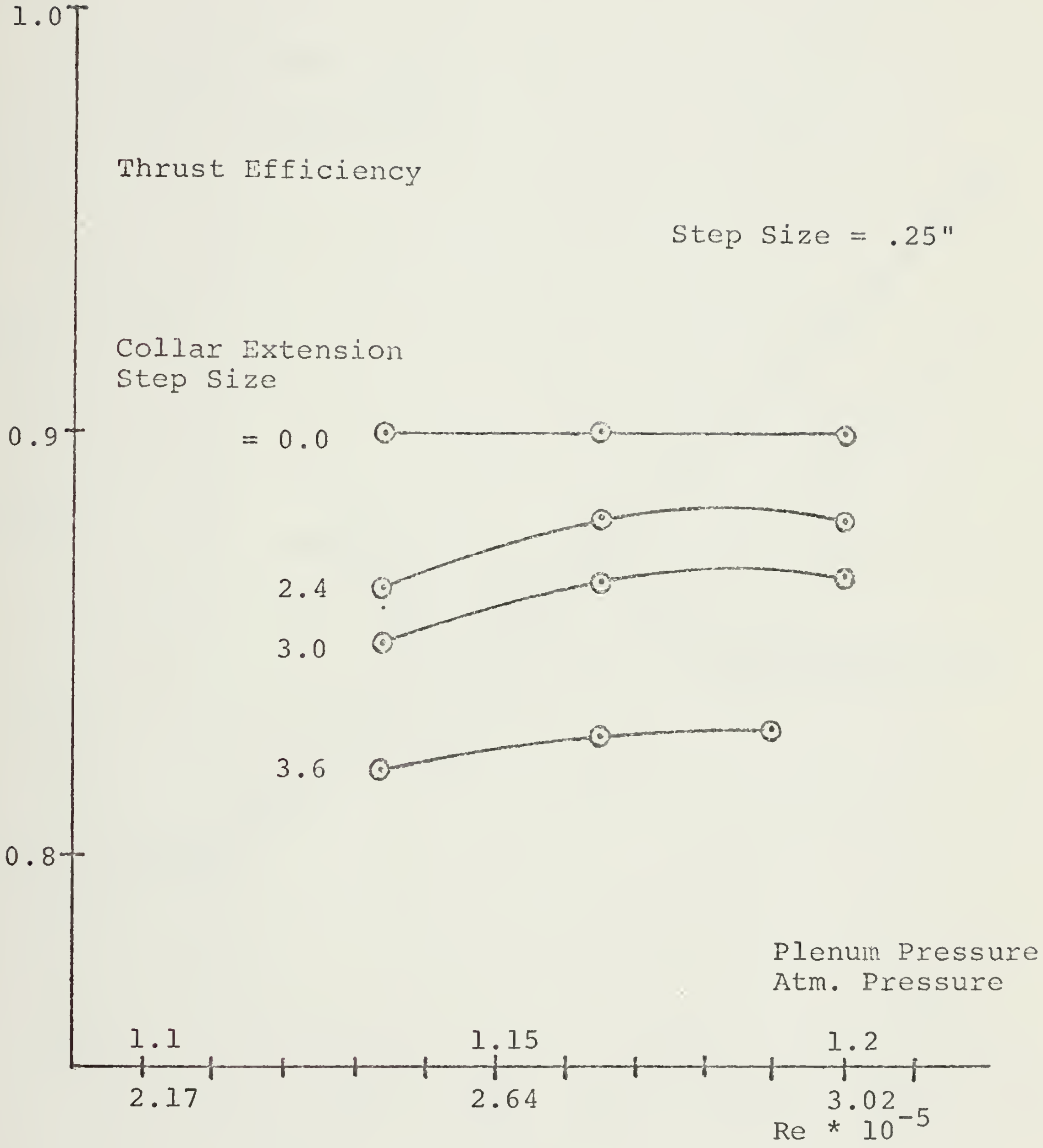

Figure 13 - THRUST EFFICIENCY RESULTS

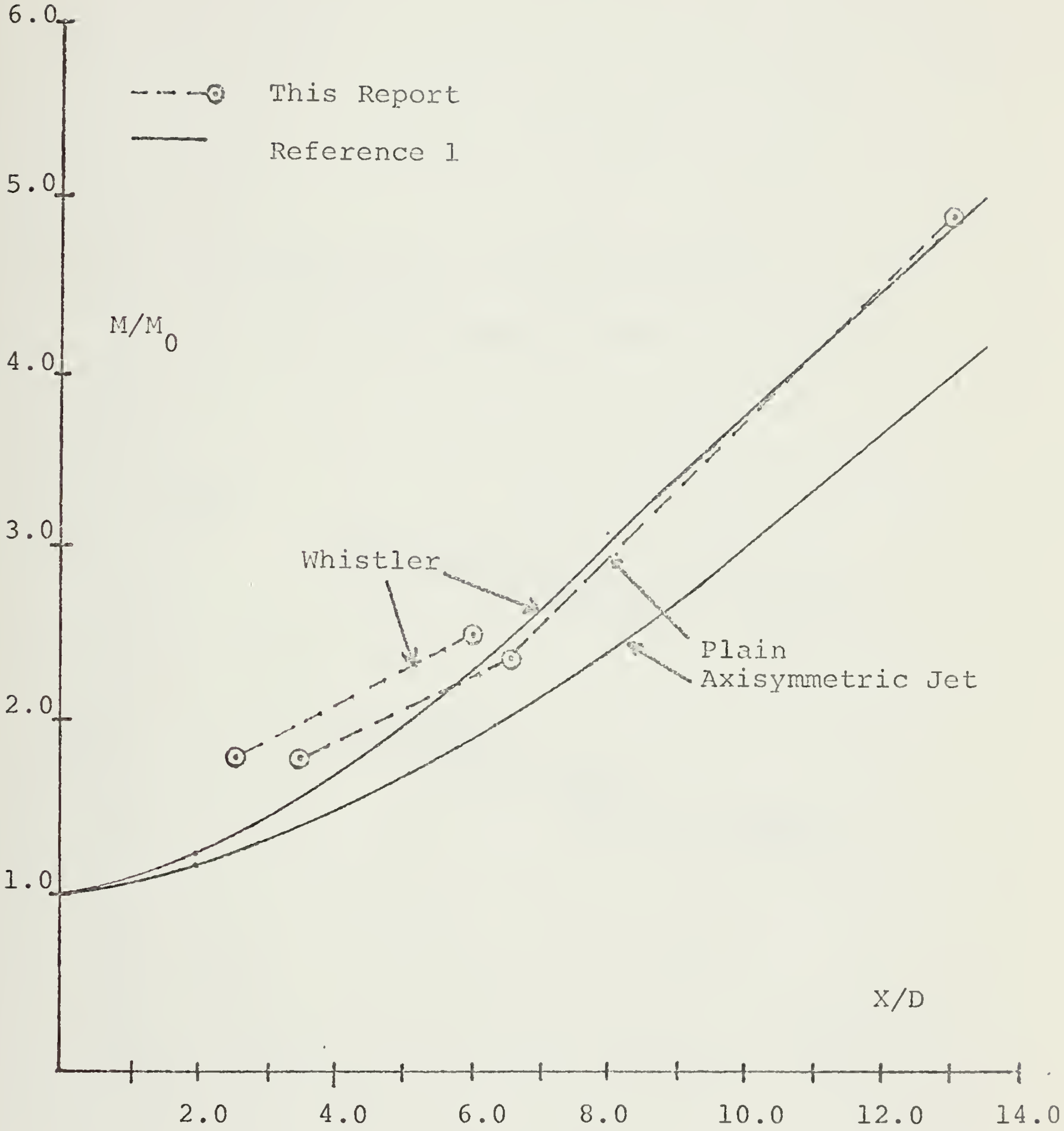

Figure 14 - ENTRAINMENT RATIO RESULTS AND COMPARISON DATA

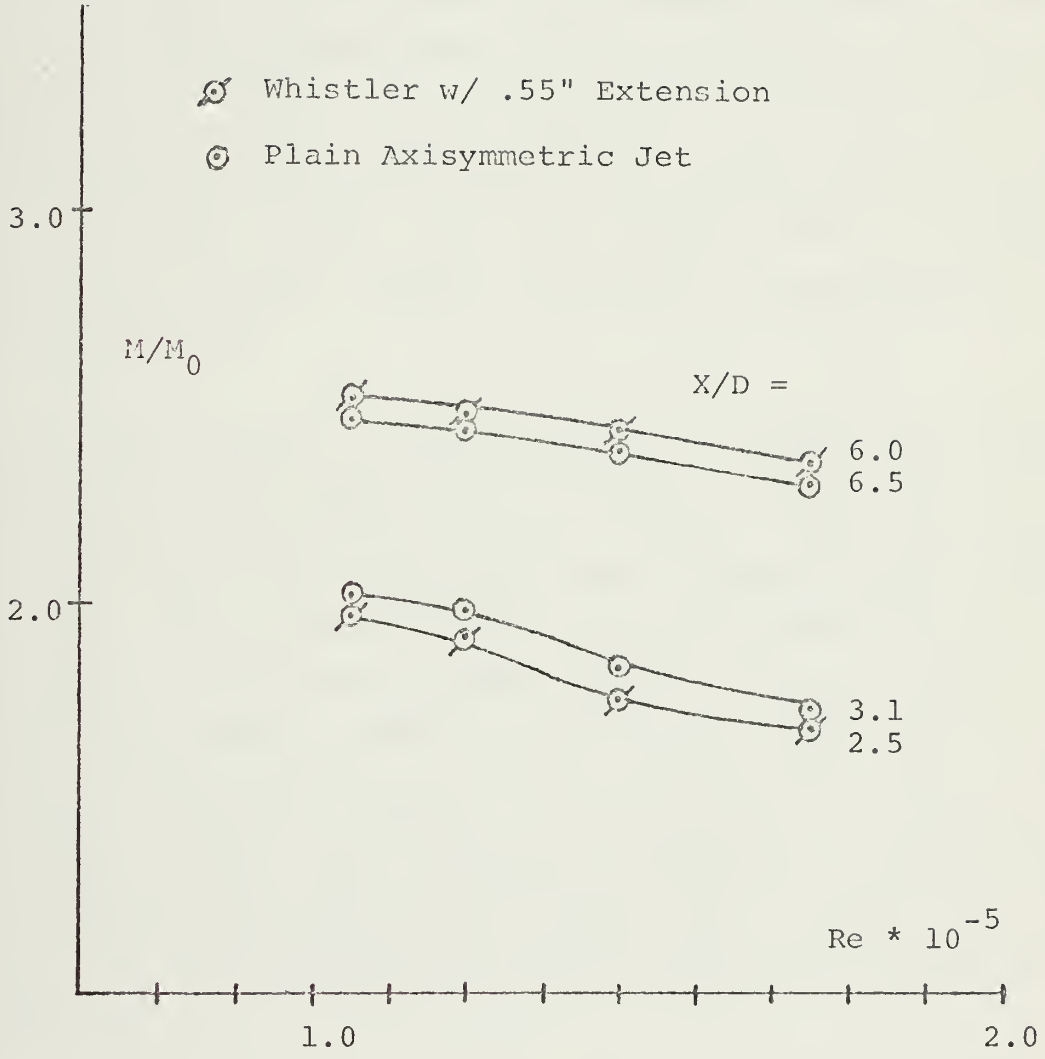

Figure 15 - ENTRAINMENT RATIO VS REYNOLDS NUMBER

Lack of time precluded testing at more jet axial locations, as each location required a different orifice cylinder (see appendix A). Of the original four orifice cylinders constructed using reference 8 data, only two were useable as the spreading angles encountered averaged about 28 degrees, or 10 degrees less than those used in reference 8. In order to be effective, the orifices had to be positioned at axial distances further than they were designed for. One of those was modified to obtain readings at its design position, also. The larger two were never effective. Another problem encountered was the mass flow limitation of the porous cylinder air supply. This restricted the useable nozzle flow at axial locations beyond X/D of about 6 to such low values that a whistler oscillation strong enough to affect the entrainment could not be produced.

It was hoped that high speed motion pictures would be taken of the tuft experiment; however, this phase of the photographic experiments was not reached. The effectiveness of the tufts in indicating the circumferential collar positions of attached and detached flow was proven in the high-speed still picture phase. Motion pictures with a 64 frame per second camera showed that a much higher speed camera was necessary to slow the motion such that motion pictures would be useful in slowing the tuft motion to a reasonable speed. The necessary film speed was estimated as about 800 frames per second; however, the pictures were never taken. Some representative still pictures are presented in figure 16.

Lampblack tests appeared to be productive as indicators of the general behavior of the collar attachment point. Indications are that a sort of Coanda effect is involved, modified by the fact that while the jet is attached at any

point on the collar there are other points where detached flow allows a backflow into the collar jet gap, which tends to relieve the Coanda effect causing a circumferential shift in the point (or points) of attachment. At a fixed collar extension, with increasing jet velocity, the attachment point was observed to move upstream to a limiting position, just as the Coanda jet described in reference 10. However, at fixed exit velocity and increasing collar extension a different behavior was observed. The attachment point seemed to move with the collar until a point was reached at which the frequency of oscillation jumped. At that instant the point of attachment also appeared to jump suddenly back to its original position relative to the jet exit. This behavior indicated some interdependence of the whistler attachment phenomenon and the oscillation phenomenon.

In addition to the above experiments, two other observations were made which verified those of Hill and Greene.

First, it was noted that extension of the whistler collar seemed to increase mass flow through the nozzle.

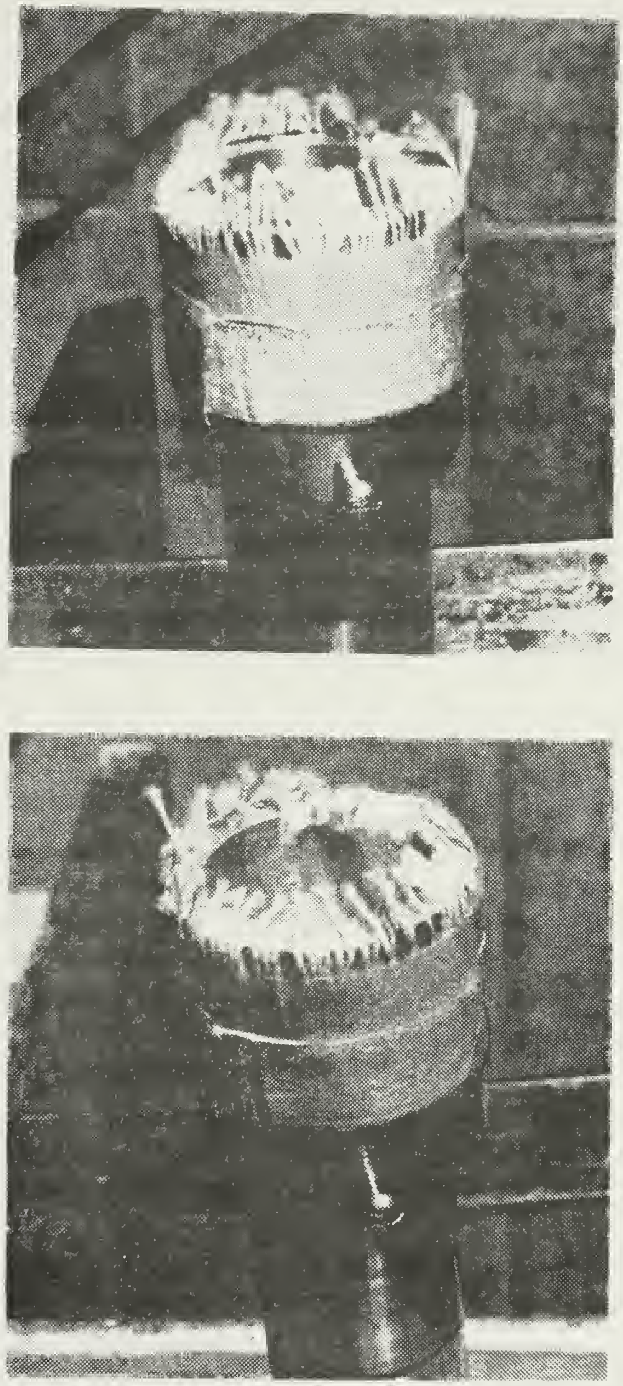

Figure 16 - TUFT PICTURES, RESULTS

This was confirmed with static pressure measurements in the nozzle 'throat'. These indicated that the collar was acting as an overexpanded diffuser, resulting in an effective exit area slightly greater than the 'throat' cross section but less than the collar cross section, and further resulting in a greater mass flow through the nozzle.

Second, it was noted that a correspondence between frequency of oscillation, jet exit velocity, and collar extension seemed to exist. It was found that by gradually extending the collar as plenum pressure was increased, one could 'follow' a frequency of oscillation. Accordingly, collar extensions were measured and jet velocity calculated at fixed frequencies of oscillation, and it was found that these fixed frequencies corresponded to constant ratios of collar extension to jet velocity, thus confirming the organ pipe character of the whistler oscillation noted by Hill and Greene.

VII. CONCLUSIONS AND RECOMMENDATIONS

The thrust efficiency and mass entrainment characteristics of the whistler nozzle have been measured, in the case of the entrainment, using a technique heretofore not used on an unsteady jet. Further, observations have been made which should contribute to a further understanding of the whistler flow mechanism.

Several directions of further work are indicated. First, it is recommended that a thrust measurement device using a pendulum arrangement, similar to that used in reference 15, be constructed for a more accurate determination of the whistler efficiency. A device of this type might avoid the hysteresis problems encountered with low thrusts on a conventional thrust bed. It is also recommended that a whistler nozzle of smaller throat diameter be constructed to permit mass entrainment measurements , at further jet axial locations, in the entrainment chamber, at the high exit velocities required to produce a strong oscillation. This will also permit further study of the possibility of whistler measurements in the chamber over a greater range of Reynolds number. Next it is recommended that further flow visualization experiments be conducted. Specifically, high speed motion pictures of the tufts used here, and high speed schlieren photography of the jet, should prove useful. Finally, it is recommended that other unsteady nozzles be tested in the chamber, as the poor results obtained here with the whistler are only preliminary and may not be indicative of the usefulness of the chamber with non-acoustic effects such as swirl.

VIII. INTRODUCTION- THE RING WING

The present work concerns a hollow cylinder, axially aligned, in supersonic flow and undergoing small amplitude oscillations in angle of attack. The intent is to calculate the resulting pressure distributions and aerodynamic moments on what might be more properly termed a ring wing.

Previous investigations, i.e. references 12 and 13, have applied the method of characteristics towards the separate calculation of the inner and outer flowfields, as well as pressure distributions and generalized aerodynamic forces, for such a cylinder in supersonic flow whose walls are undergoing small amplitude sinusoidal oscillations, or panel flutter. These previous investigations resulted in computer programs to perform the necessary calculations.

The primary thrust of the present work was the modification of the previously created programs and then the combination of their results to calculate the unsteady pressure distribution, lift and moment on the cylinder undergoing angle of attack oscillations. Finally, using the modified programs, a parametric study of these items was conducted.

IX. PROBLEM FORMULATION

This development is closely based on several previous papers , i.e. references 12 and 13.

Consider a circular cylindrical shell, in supersonic, inviscid, adiabatic flow, whose axis is aligned with the freestream, and which is undergoing small amplitude oscillations in angle of attack, about the Z axis.(figure 17)

The governing equation for this flow situation is the linearized unsteady potential equation, in cylindrical coordinates.

$$(1-M^2)\ \Phi_{xx} + \Phi_{rr} + \frac{1}{r}\ \Phi_r + \frac{1}{r^2}\ \Phi_{\theta\theta} - \frac{2M}{c}\ \Phi_{xt} - \frac{1}{c^2}\ \Phi_{tt} = 0$$

The relevant boundary conditions are the flow tangency condition and Sommerfeld's radiation condition, i.e.,that disturbances will propagate away from their source.

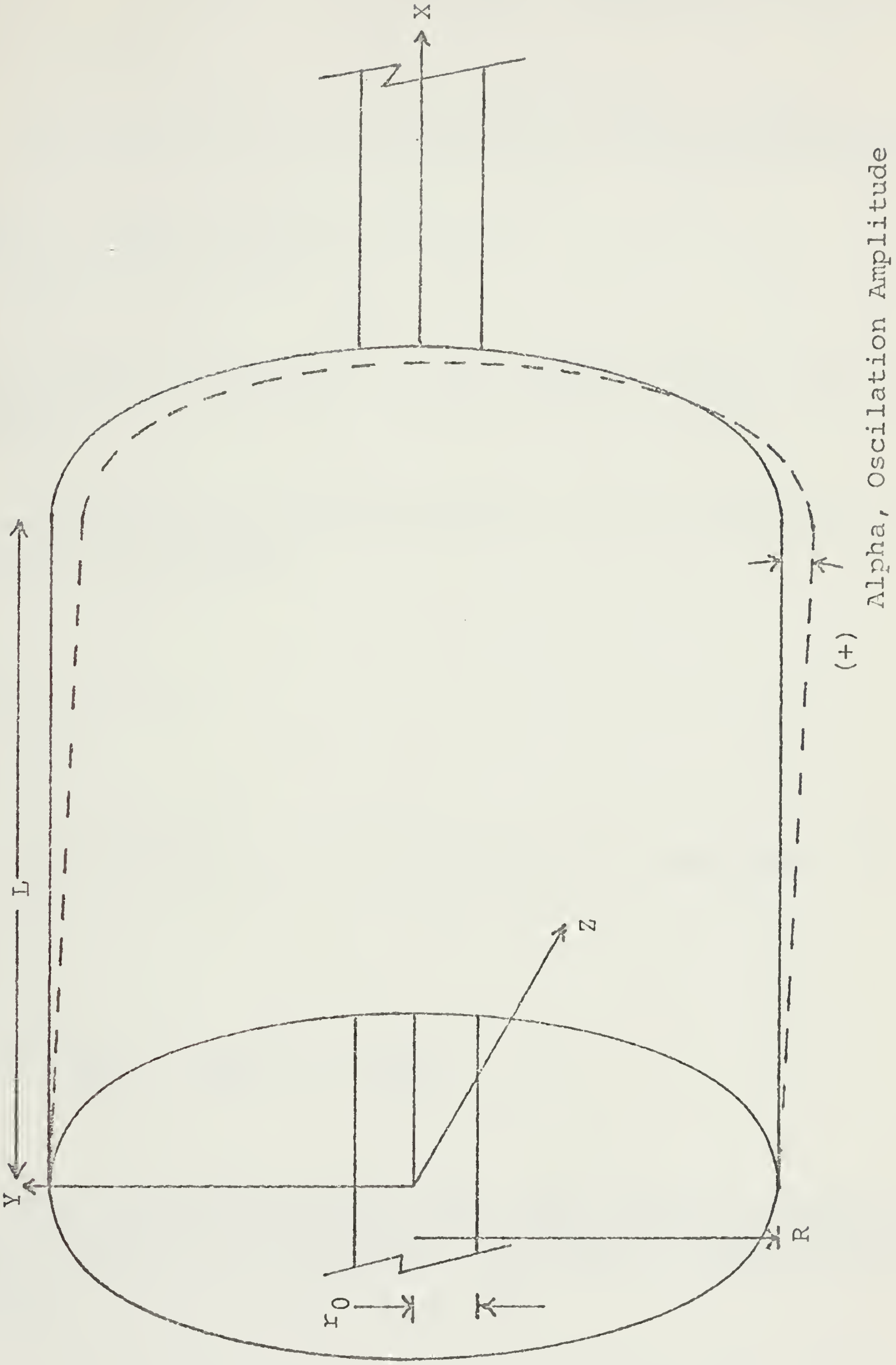

Figure 17 - RING WING ILLUSTRATION

One further condition is necessary, along the X-axis, which amounts to setting the pressure disturbance at the axis equal to zero.

The linearized form of the flow tangency condition is:

$$\Phi_r\Big|_{r=R} = \frac{\partial h}{\partial t} + U_\infty \frac{\partial h}{\partial x} \,, 0 \leqslant x \leqslant L$$

which must be satisfied on the cylinder inner and outer surface.

As stated, the boundary condition at the axis is a zero pressure disturbance:

$$C_p\Big|_{r=0} = 0$$

The linearized form of the pressure coefficient is as follows:

$$C_p = \frac{-2}{U_\infty^2} \Phi_t - \frac{2}{U_\infty} \Phi_x = \frac{P - P_\infty}{q_\infty}$$

After nondimensionalization, using cylinder length and length divided by freestream velocity, the above equations become:

$$(1-M^2)\,\phi_{xx} + \phi_{rr} + \frac{1}{r}\,\phi_r + \frac{1}{r^2}\,\phi_{\theta\theta} - 2M^2\,\phi_{xt} - M^2\,\phi_{tt} = 0$$

$$C_p = -2(\,\phi_t + \phi_x\,)$$

subject to:

$$\phi_r\Big|_{r=R} = \frac{\partial h}{\partial t} + \frac{\partial h}{\partial x} \quad ,0 \leqslant x \leqslant 1.$$

One now assumes a cylinder oscillation of the form:

$$h(x,\theta,t) = Z(x)\,\cos(\theta)\,e^{ikt}$$

where the nondimensional frequency, k, is:

$$k = \frac{\omega\,l}{U_\infty}$$

The deflection amplitude, Z(x), for the case under consideration, is of the form:

$$Z(x) = \alpha(\,x - x_o\,)$$

Following the assumed form of the deflection, the perturbation potential must be of the form:

$$\phi(x,r,\theta,t) = \phi(x,r)\cos(\theta)\, e^{ikt}$$

and, after substitution, the basic equations become:

$$(1-M^2)\,\phi_{xx} + \phi_{rr} + \frac{1}{r}\,\phi_r + \frac{(k^2M^2-1\ )}{r^2}\,\phi - i2kM\,\phi_x = 0$$

$$C_p = -2(\ \phi_x + ik\phi\ )$$

subject to:

$$\phi_r\Big|_{r=R} = Z_x + ikZ \quad ,o \leqslant x \leqslant 1.$$

and:

$$C_p\Big|_{r=0} = 0$$

X. METHOD OF CHARACTERISTICS

For supersonic flow, the linearized perturbation potential equation is hyperbolic, and has characteristics which satisfy the following differential equation:

$$(M^2-1)\, d^2r - d^2x = 0$$

Since the characteristics in supersonic flow correspond to the Mach lines, then for ds, the differential arc length along a characteristic:

$$\frac{dr}{ds} = \pm \frac{1}{M} \qquad , \qquad \frac{dx}{ds} = \frac{\sqrt{M^2-1}}{M}$$

An arbitrary function, F(x,r), has the following derivatives along the characteristics:

$$\frac{dF}{ds} = F_x \frac{dx}{ds} + F_r \frac{dr}{ds} = \frac{\sqrt{M^2-1}}{M} F_x \pm \frac{1}{M} F_r$$

Defining ds1 and ds2 to be the differential arc lengths along the left, and right-running Mach lines respectively, then:

$$F_1 = \frac{dF}{ds_1} \qquad , \qquad F_2 = \frac{dF}{ds_2}$$

The cross derivatives become:

$$-F_{12} = -F_{21} = \frac{1}{M^2}((1-M^2)\ F_{xx} + F_{rr})$$

Solving now for Fx and Fr:

$$F_x = \frac{M}{2\sqrt{M^2-1}}\ (F_1 + F_2)$$

$$F_r = \frac{M}{2}\ (F_1 - F_2)$$

Now the basic equations may be written in terms of ϕ and its derivatives along the characteristics as follows:

$$\phi_{12} = \phi_{21} = \frac{1}{2rM}\ (\phi_1 - \phi_2) + (k^2 - \frac{1}{r^2M^2})\ \phi - \frac{ikM}{M^2-1}\ (\phi_1 + \phi_2)$$

$$\phi_r = \frac{M}{2}\ (\phi_1 - \phi_2) = Z_x + ikZ$$

$$C_p = -2(\phi_x + ik\phi)$$

These equations have been put into finite difference form and programmed in Fortran IV for the separate cases of exterior flow and interior flow of a cylinder whose walls were undergoing small amplitude sinusoidal oscillations. In the interior flow program the X axis boundary condition is satisfied on a small inner cylinder in place of the axis, to circumvent problems encountered should r go to zero. For detailed accounts of the equations and programs refer to references 12 and 13.

The primary work here was the transformation of the aforementioned programs to the case under consideration , i.e., a cylinder undergoing small amplitude oscillations in angle of attack, and then a parametric variation study of the pressure distributions and generalized aerodynamic force. The programs were modified such that all cases run were with an angle of attack amplitude of 0.1 radians. Since the basic equation is in a linearized form, the conversion of any results to other angle of attack amplitudes is a simple matter of multiplication. For those interested, the programs resulting from changes required to the reference 12 and 13 programs are listed in appendix D.

XI. GENERALIZED AERODYNAMIC FORCE

As stated above, the results studied were the pressure coefficient amplitude distribution, and the generalized aerodynamic force, Qmr. In its most general form, Qmr is as follows:

$$Qmr = \frac{1}{2} \int C_{Pm} \Psi_r(x)\ dx$$

$$Z(x) = \sum_j A_j \Psi_j(x)$$

where Cpm is the pressure coefficient amplitude resulting from the m'th axial deflection mode, PSIr is the r'th axial deflection mode, and A is the amplitude of the j'th axial deflection mode. For the special case under consideration, Q takes the following form:

$$Q = \frac{1}{2} \int C_p \Psi(x)\ dx$$

$$Z(x) = \Psi(x) = \alpha(x - x_0)$$

Thus , in the case under study Q has the special interpretation of being the moment coefficient amplitude about the point Xc multiplied by the angle of attack amplitude, alpha, which is equal to 0.1 radians in all cases presented .

XII. RESULTS AND DISCUSSION

Several cases of comparison were considered towards the evaluation of program results. Figure 18 presents two cases of comparison for pressure distributions. The outer radius-to- length ratio was taken to such a value (10) as to approximate a flat plate locally. The inner radius-to-length ratio was taken to such a value (9.75) as to cause a reflection on the inner surface of the outer cylinder.

For sufficiently large radius - to - length ratios the exterior pressure distribution should approximate the theoretical value for a flat plate in supersonic flow, i.e. $2\alpha/\beta$. Figure 18A presents this comparison, and as can be seen agreement is good.

For sufficiently large radius - to - length ratios the interior pressure distribution should approximate the theoretical value for a flat plate. Additionally, if the inner cylinder is of such a radius-to-length ratio as to cause a Mach wave to reflect upon the outer cylinder inner surface, a flow situation exists which should approximate a flat plate in a free jet, where the mach waves are reflected from the jet boundary. This is due to the boundary condition imposed on the inner cylinder, Cp = 0. Reference 16 has treated this case in analytic form for small frequencies. Figure 18, A and B, presents a comparison of program results and the results of reference 16. As can be seen agreement is good.

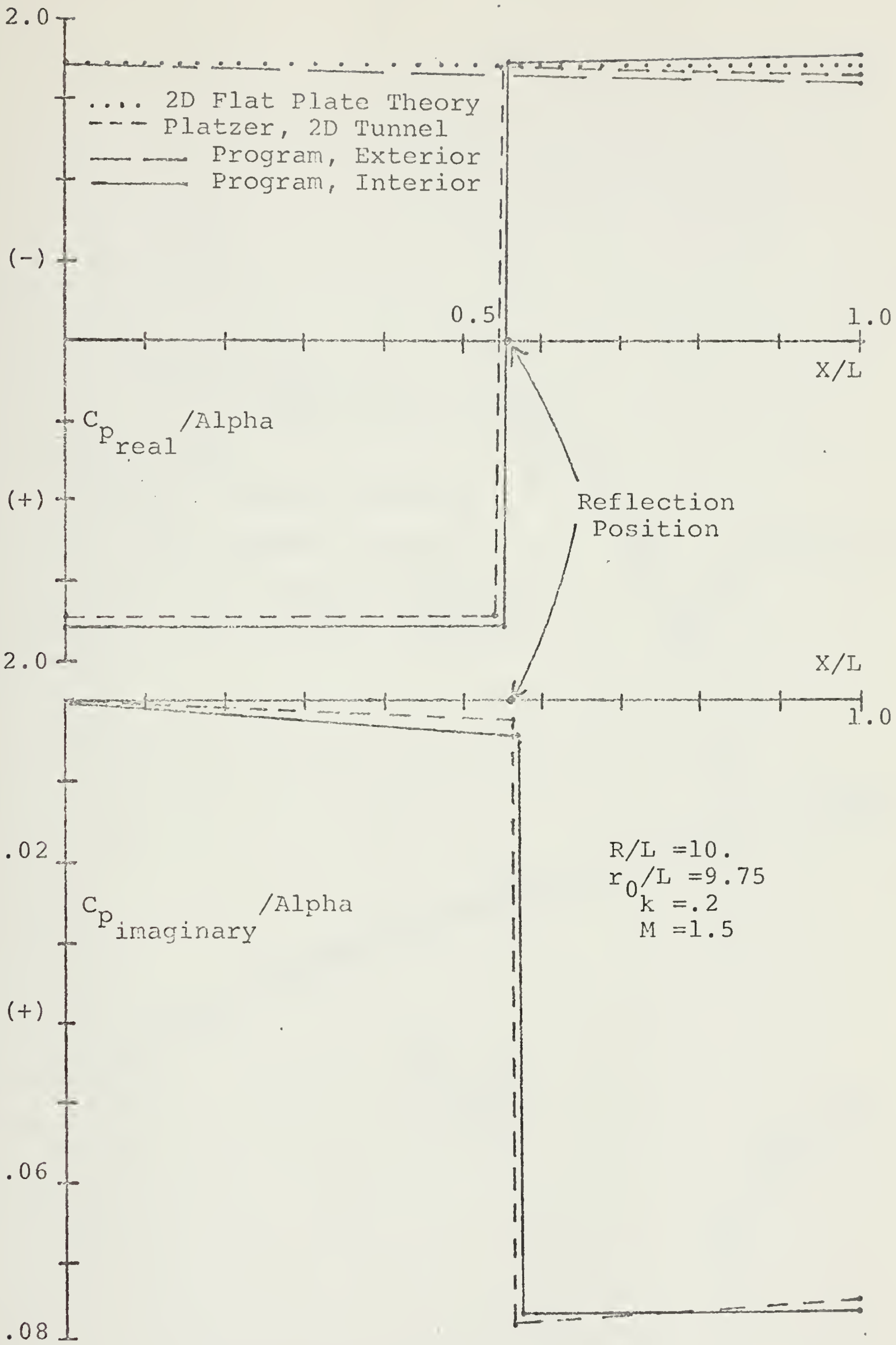

Figure 18 - AXIAL PRESSURE DISTRIBUTION, 2D LIMITING CASE

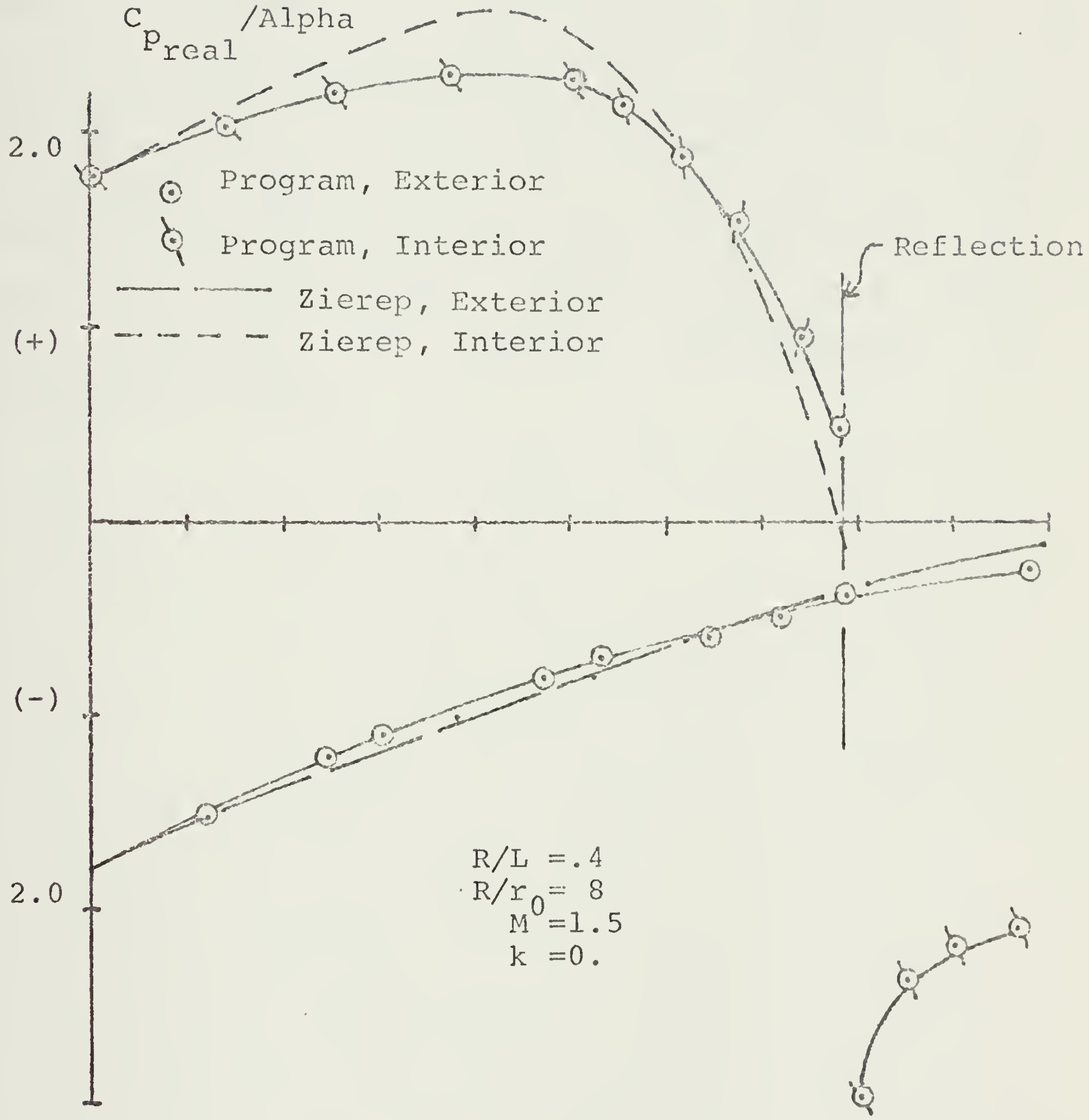

Figure 19 - AXIAL PRESSURE DISTRIBUTION, COMPARISON WITH ZIEREP

Reference 14 has treated the case of a nonoscillating ring wing in supersonic flow. Figure 19 presents a comparison of program results and those of reference 14, for the case shown. As can be seen agreement is fair.

In reference 12, which developed the basic inner flow field program used in this report, the occurrence of a numerical instability in the pressure distributions, under certain conditions, was noted. It was found that this disturbance, which occurred only after a reflection, was due to an undefined constant in the subroutine which computed the boundary condition at the axis. After defining the constant correctly, the pressure distributions were seen to settle down quite nicely. Figure 20 presents a before and after comparison of pressure distributions for a representative case.

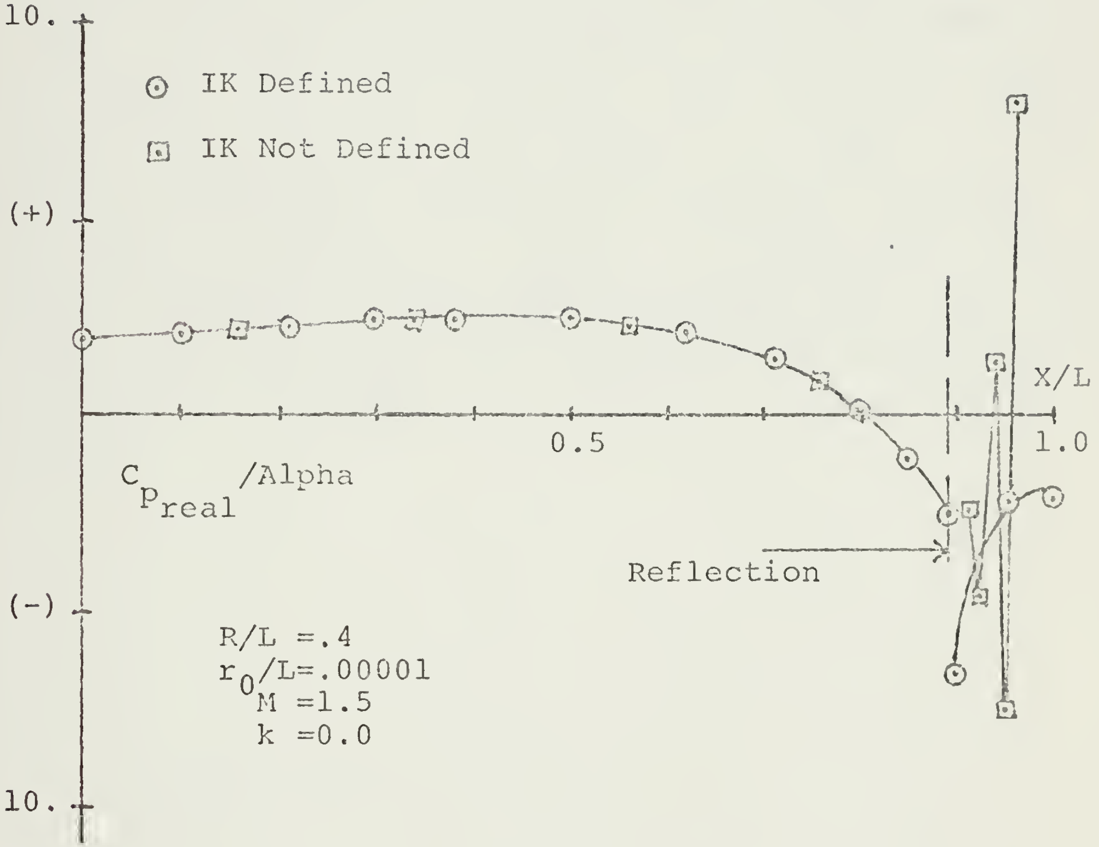

Figure 20 - NUMERICAL INSTABILITY ILLUSTRATION

Figures 21 through 23 present various parametric studies of the moment coefficient, Q, for cases both with and without a reflection on the inner cylinder surface. In these figures the coefficient plotted is actually the difference between that calculated for the inner cylinder surface and that calculated for the outer cylinder surface, divided by the angle of attack amplitude. Thus the coefficients plotted are total moment and pressure coefficients, as opposed to those plotted earlier, which are the coefficients for the inner and outer cases separately. As can be seen from figure 22,for a center of rotation at the leading edge the cylinder has definite geometric regions of stability with respect to angle of attack. Figure 21 illustrates the effect of increased frequency on the moment coefficient. Figure 23 illustrates a typical pressure distribution including one reflection, from which one can infer the reason for the behavior of Q in figure 22, and also the behavior of Q with a varying center of rotation.

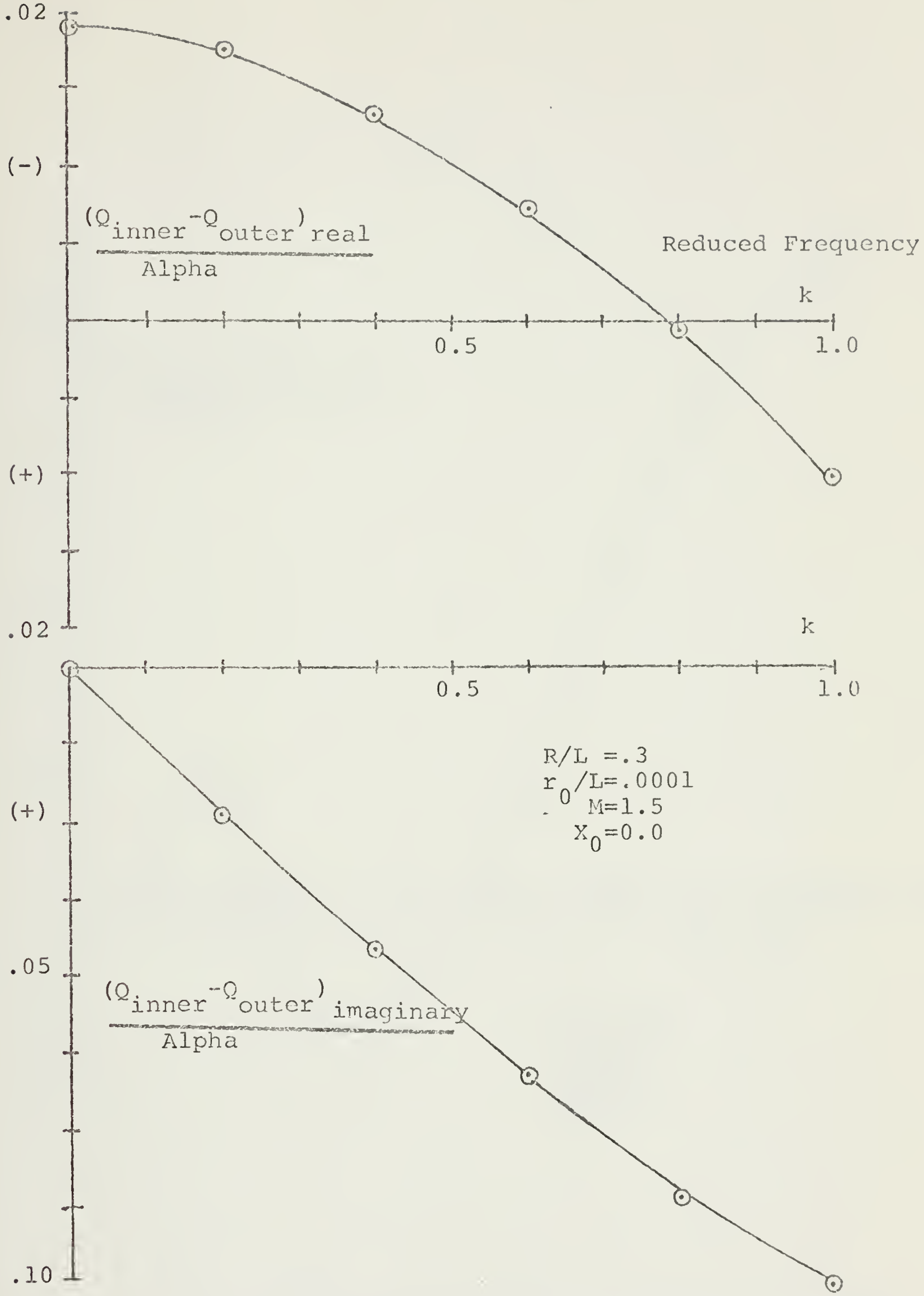

Figure 21 - PITCHING MOMENT VS REDUCED FREQUENCY

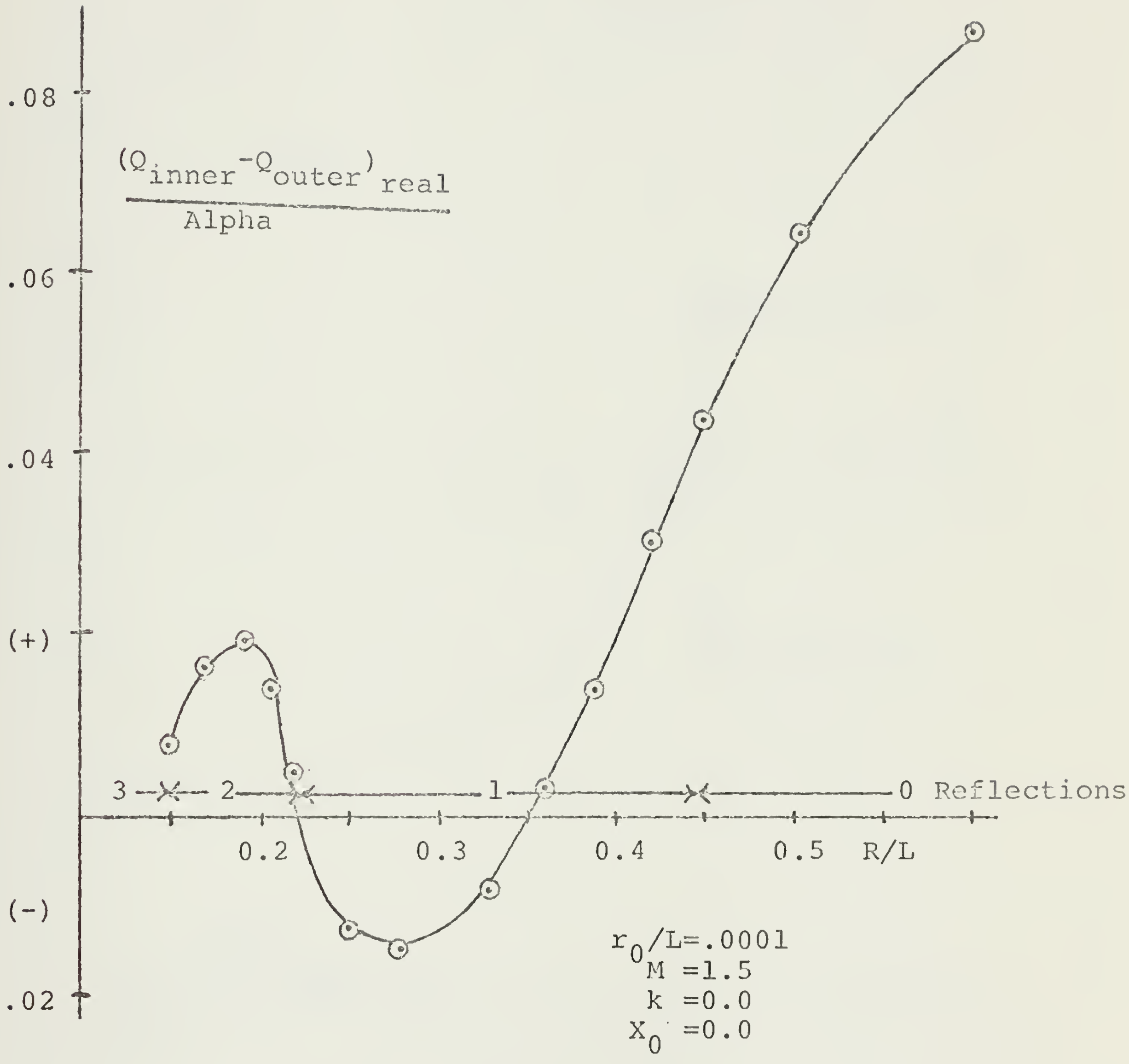

Figure 22 - PITCHING MOMENT VS OUTER RADIUS-TO-LENGTH RATIO

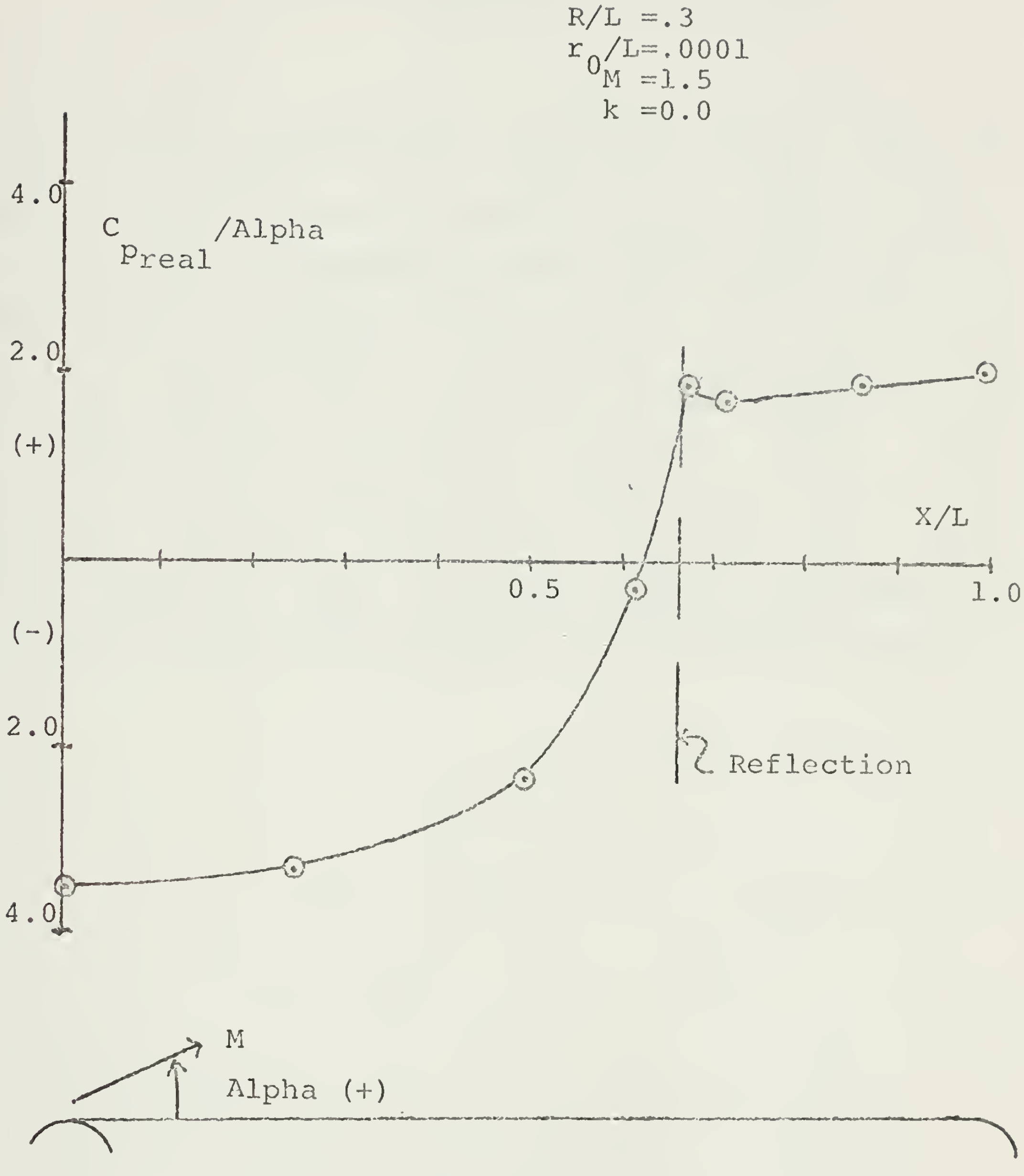

Figure 23 - REPRESENTATIVE AXIAL PRESSURE DISTRIBUTION INCLUDING ONE REFLECTION

XIII. CONCLUSIONS AND RECOMMENDATIONS

The computer programs of references 12 and 13 have been successfully adapted to the case of a ring wing in supersonic flow undergoing oscillations in angle of attack. Available cases for comparison have shown good agreement, indicating the validity of the method. The programs make possible the relatively easy calculation of the unsteady lifts and moments of a ring wing in supersonic flow, for such applications as tubular artillery shells (STUP, spinning tubular projectile), although spin may induce aerodynamic effects not accounted for in the method. Further evaluation and parametric studies are recommended for a more complete verification of the computer programs.

APPENDIX A

ISENTROPIC THRUST CALCULATIONS

Isentropic thrust calculations made use of standard isentropic relations. Calculations were based on plenum pressure and nozzle exit area. The formula for isentropic thrust is arrived at as follows. Nozzle thrust may be written in the following form:

$$T_s = w\ V_{ex} = (\rho A M^2 \gamma RT)_{ex}$$

where W is nozzle mass flow, A is exit area, and one has applied the speed of sound relation. Exit Mach number may be written in terms of pressure ratio as follows:

$$M_{ex} = \frac{2}{\gamma-1}\ ((P_0/P_{ex})^{\gamma-1/\gamma} -1)$$

Applying this and the state equation to the formula for Ts one obtains:

$$T_s = P_{ex}A_{ex}\ \frac{2}{\gamma-1}\ ((P_0/P_{ex})^{-1} -1)$$

Now, once one has measured plenum and ambient pressure, and thrust, Texp, one can calculate the isentropic thrust efficiency:

$$\eta = T_{exp}/\ T_s$$

APPENDIX B

ENTRAINMENT RATIO CALCULATIONS

Mass flows and entrainment ratios were calculated according to the equations and procedures set out in reference 11, the ASME Power Test Codes. The equation for mass flow, from reference 11 is:

$$w = 359\ c\ f\ d^2\ Fa\ Y\ \sqrt{h\rho} \quad ,\text{lb/hr}$$

where:

c Discharge Coefficient

f $=1/\sqrt{1-\beta^4}$ $\beta = d/D$

d and D

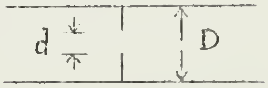

Fa Thermal Expansion Factor

Y (Ya for a venturi) Adiabatic Expansion Factor

h The pressure drop across the device, in inches of water

ρ Density of the fluid being metered, pounds per cubic foot

If w1 is the entrained flow and w2 the primary, then (w1 uses a venturi, w2 an orifice):

$$\frac{w_1}{w_2} = \frac{c_1}{c_2}\ \frac{f_1}{f_2}\ \frac{(d_1)^2}{d_2}\ \frac{Fa_1}{Fa_2}\ \frac{Ya_1}{Y2}\ \sqrt{\frac{h_1}{h_2}}$$

Non-geometric factors for the primary flow, such as discharge coefficient, could be reasonably approximated for all tests as:

$C2=.65 \qquad Fa2=1.0 \qquad Y2=.99$

In the case of the entrained flow these factors had to be changed for each test axial location, due to the widely varying flow requirements. The geometric factors above had the following fixed values:

$F1=1.0328 \quad d1=.75 \qquad F2=1.0792 \quad d2=1.11$

Now, entrainment ratio is commonly written as:

$$\frac{M}{M_0} = \frac{w_1 + w_2}{w_2} = \frac{w_1}{w_2} + 1$$

Using the previous formula for w1/w2, the entrainment ratio may now be written as:

$$\frac{M}{M_0} = A\sqrt{\frac{h_1}{h_2}} + 1$$

where A is the combination of the ratios of factors previously listed. This equation was used to calculate the nozzle entrainment ratios.

APPENDIX C

ENTRAINMENT CHAMBER DESIGN

The entrainment chamber design was closely based on previous work by Ricou and Spalding (reference 7), and Peschke (reference 8). Peschke's report especially was a good source of specific design data, while Ricou and Spalding was primarily a source of the design principles.

The entrainment chamber consisted essentially of a central porous cylinder, closed at one end with a solid wall through which the nozzle protruded, the other end being open to the outside. Orifice plates of specific diameters were constructed and mated to cylinders of specific length, length and diameter specified according to the data available in Peschke. These orifice cylinders were of such outside diameter that they fit closely inside the porous cylinder, into which they were inserted for the measurement of mass flow at the various jet axial positions corresponding to the orifice diameters. The purpose of the orifice was to seal the open end such that entrained air could only enter through the porous cylinder. The purpose of the orifice cylinder was to seal off that portion of the porous cylinder beyond the jet axial position where flow was being measured. The porous cylinder was surrounded everywhere, except at the open end, by a box, also encasing the nozzle plenum, which served as the membrane air supply.

The entrainment chamber was about 4 by 4 feet square and 4 feet high, supported on 3 foot legs. The porous cylinder

was 30 inches in diameter and 25 inches long. Orifice diameters used, corresponding to the listed jet axial positions, were as follows:

Diameter	X/D
1.75	2.5
3.0	5.0
6.5	13.0

The entrainment chamber box, legs, orifice plates and porous cylinder frame work were all constructed of wood. The orifice cylinders were made of fiberglass sheet and the porous covering to the porous cylinder frame work was two layers of dacron crepe cloth, as suggested in Peschke's report.

One critical chamber design parameter was orifice diameter. It is clear that too small an orifice would interfere with the jet being measured, while too large an orifice would not properly restrict the entrained flow to entering only through the membrane, thus preventing the creation of a readable pressure gradient across the orifice. The approach to this problem in both references 7 and 8 was to find an optimal orifice size at a specific jet axial location by testing several orifice sizes. To minimize orifice construction, this investigation took a different approach. That was to use the reference 8 orifice data as a starting point, and vary the orifice axial location, such that a readable pressure gradient was created while not interfering with the jet. In both approaches the attempt is to optimize the orifice diameter, jet axial location combination.

One primary difference between this chamber's geometry and that of others (references 7 and 8) should be noted. As shown in figure 8, exit orifices were positioned in the porous cylinder at various distances from the nozzle. That portion of the porous cylinder extending above the orifice plate was sealed by a fiberglass cylinder attached to the orifice. Thus in this situation, that portion of the jet beyond the orifice, and inside the porous cylinder exit, was not in a truly free jet flow situation. This was as opposed to the reference 7 and 8 configurations where the exit orifice corresponded to the exit of the porous cylinder. Thus in those experiments the jet past the orifice was in a truly free jet flow situation. The configuration used in this report was adopted in order to facilitate the measurement of mass flows at many axial locations. It was hoped that this chamber's geometry would not affect The chamber readings greatly, although some effect was to be expected.

An important problem, again with regard to the chamber orifices, concerned the measurement of the pressure differential across the orifice. Both reference 7 and 8 indicated that a measurement accuracy of .001 inches of water was required. Reference 7 used a micro manometer while reference 8 used a pressure transducer for this purpose. After the entrainment chamber was constructed experience showed that such accuracies were required. This investigation used an alchohol micro manometer which provided an accuracy of .0001 inches of manometric fluid. This accuracy was obtained through the combination of an inclined tube, hairline indicator, magnifying lens and a micrometer adjustment to indicator level.

Flow measurement devices for the primary and entrained flow were an orifice and venturi respectively. These were constructed and used according to ASME Power Test Codes

specifications (reference 11). Based on these specifications, an inclined water manometer was found to be necessary for measuring the orifice pressure drop, while a vertical mercury manometer was sufficient for the venturi.

APPENDIX D

PROGRAM LISTINGS AND DOCUMENTATION

This appendix contains basic program and input descriptions for the two programs used, from references 12 and 13. The programs also are listed in their modified form for the computation of a ring wing at angle of attack. The program statements relevant to the modification are indicated in the program listings. Also indicated in the interior flowfield program is the statement whose omission caused the numerical instability noted in reference 12.

The inner flow field program consists of 8 subroutines, and a main program which manipulates each of these. The action of each particular subroutine is indicated in the program listing. Inputs are made by way of a Fortran Namelist. The input parameters are, in proper order:

FSTRMN Free stream mach number.

RFDFRQ The reduced frequency.

RO The outer cylinder radius to length ratio.

RI The inner cylinder radius to length ratio.

NGRDFN Grid fineness, or the number of grid points taken on the first right running mach line.

N Circumferential mode number.

M Axial mode number.

M1 The m in Qmn, the generalized aerodynamic force.

IPRINT An output parameter. 0 indicates only basic output. 1 indicates output including such things as Phi and its derivatives at each flow field point.

Of the above inputs, in the modified program, the inputs N, M, and M1 must be set to 1, as the case under consideration is not panel flutter but a cylinder at angle of attack. The other inputs are arbitrary.

```
CCCCCCCCCCCCCCCCCCCCCCCCCCCCCCCCCCCCCCCCCCCCCCCCCCCCCCCCCCCCCCCCCCCCCCCC
C                                                                      C
C            CYLINDRICAL SHELL/PANEL FLUTTER PROGRAM                   C
C                                                                      C
CCCCCCCCCCCCCCCCCCCCCCCCCCCCCCCCCCCCCCCCCCCCCCCCCCCCCCCCCCCCCCCCCCCCCCCC
C
C                    THIS IS THE MAIN PROGRAM
C
      COMPLEX PHI(400),DPHIS1(400),DPHIS2(400)
      DIMENSION X(400),R(400),XPT(400),CPR(400),CPI(400)
      DIMENSION DUMMY(400),DUNCE(400)
      COMMON/BLCK1/ FSTRMN,DELTAS,DX,DH,DSTSTR,RO,RI,REDFRQ
      COMMON/BLCK2/ A1,A2,A3,A4,RN,RM,RM1,FACT1,FACT2
      COMMON/BLCK3/ NGRDFN,NPTS,LCOUNT,IHAVEP,N,M,M1,IPRINT
      COMMON/BLCK4/ PHI,DPHIS1,DPHIS2
      COMMON/BLCK5/ X,R,XPT,CPR,CPI
      DATA PI/3.141593/
C
      ENDPT(Y2,Y1,X0,X2,DELX) = ( Y2 - Y1 )*( X0 -X2 )/DELX
     1   + Y2
C
      EPS = 1.E-04
      IER = 0
      CALL INPUT(IER)
      IF ( IER .EQ. 1 ) GO TO 12
 1000 CONTINUE
C
      IHAVEP = 1
      LCOUNT = 1
C
      CALL INITAL
C
    1 CONTINUE
C
      CALL COMPXR
C
C     IS THE GRID POINT ON THE INITIAL RIGHT RUNNING MACH
C     LINE?
C
      IF (( LCOUNT .EQ. 1 ) .AND. (IHAVEP .LE. NGRDFN ))
     1   GO TO 3
C
C     IS THE GRID POINT ON THE OUTER CYLINDER SURFACE?
C
      IF ( IHAVEP .EQ. 0 ) GO TO 5
C
C     IS THE GRID POINT ON THE INNER CYLINDER SURFACE?
C
      IF ( IHAVEP .EQ. NGRDFN ) GO TO 6
C
C     THEN THE GRID POINT IS IN THE GENERAL FLOW FIELD.
C
    2 CALL GENFPT(IER)
      IF ( IER .EQ. 1 ) GO TO 12
      IHAVEP = IHAVEP + 1
      GO TO 1
C
    3 CALL MACHLN
      IF ( IHAVEP .EQ. NGRDFN ) GO TO 4
      IHAVEP = IHAVEP + 1
      GO TO 1
C
C     THIS IS THE LAST POINT ON THE INITIAL MACH LINE.
C
    4 LCOUNT = LCOUNT + 1
      IHAVEP = 0
      GO TO 1
C
    5 CALL RAD2
C
C     IS THIS GRID POINT PAST THE FLEXIBLE CYLINDER LENGTH?
C
```

```
      IF ( (X(1)+EPS) .GE. 1. ) GO TO 8
      IHAVEP = IHAVEP + 1
      GO TO 1
C
    6 CALL RAD1
      IHAVEP = 0
      LCOUNT = LCOUNT + 1
      GO TO 1
C
    8 CONTINUE
      IF ( ABS(XPT(LCOUNT) - 1. ) .LE. EPS ) GO TO 10
      L = LCOUNT
      LM1 = LCOUNT - 1
      LM2 = LCOUNT - 2
      XPT(L) = 1.
      CPR(L) = ENDPT(CPR(LM1),CPR(LM2),1.00,XPT(LM1),DSTSTR)
      CPI(L) = ENDPT(CPI(LM1),CPI(LM2),1.00,XPT(LM1),DSTSTR)
C
C
      WRITE(6,105)
      DO 9 I = 1,L
      ARG = RM1*PI*XPT(I)
C                                                          C
C     THE FOLLOWING TWO CARDS WERE MODIFIED FROM THE       C
C     ORIGINAL REFERENCE 12 PROGRAM.                       C
C                                                          C
      DUMMY(I)=CPR(I)*.1*XPT(I)
    9 DUNCE(I)=CPI(I)*.1*XPT(I)
C
      SUM1 = 0.5*(CPR(L) + CPR(LM1))*(1.00 - XPT(LM1))
      SUM2 = 0.5*(CPI(L) + CPI(LM1))*(1.00 - XPT(LM1))
C
      WRITE(6,114) FSTRMN,REDFRQ,RO,RI,N
C
      CALL QSF(DSTSTR,DUMMY,DUMMY,LM1)
      CALL QSF(DSTSTR,DUNCE,DUNCE,LM1)
      QREAL = 0.5*(DUMMY(LM1) + SUM1)
      QIMAG = 0.5*(DUNCE(LM1) + SUM2)
C
      WRITE(6,115) M,M1,QREAL,M,M1,QIMAG
      GO TO 12
C
   10 CONTINUE
      XPT(L) = 1.
      WRITE(6,105)
      DO 11 I = 1,LCOUNT
      ARG = RM1*PI*XPT(I)
      DUMMY(I)=CPR(I)*.1*XPT(I)
   11 DUNCE(I)=CPI(I)*.1*XPT(I)
C
      WRITE(6,114) FSTRMN,REDFRQ,RO,RI,N
C
      CALL QSF(DSTSTR,DUMMY,DUMMY,L)
      CALL QSF(DSTSTR,DUNCE,DUNCE,L)
      QREAL = 0.5*DUMMY(L)
      QIMAG= 0.5*DUNCE(L)
      WRITE(6,115) M,M1,QREAL,M,M1,QIMAG
C
   12 CONTINUE
      WRITE(6,998)
 998  FORMAT('1','CP REAL')
      CALL PLOTP(XPT,CPR,LCOUNT,0)
      WRITE(6,999)
 999  FORMAT('1','CP IMAGINARY')
      CALL PLOTP(XPT,CPI,LCOUNT,0)
      STOP
  150 FORMAT(F10.5)
  105 FORMAT('1',T19,'I',T27,'X',T38,'CPR',T50,'CPI',//)
  110 FORMAT('0',15X,I5,3(3X,F9.5))
  114 FORMAT(//' ',T20,'MACH NUMBER = ',F10.7,//' ',T20,
     1   'REDUCED FREQUENCY = ',F10.7,/' ',T20,'(RADIUS/',
     2   'LENGTH) OUTER = ',F10.7,/' ',T20,'(RADIUS/LENGTH)'
```

```
     3   ,' INNER = ',F10.7,/' ',T20,'CIRCUMFERENTIAL MODE',
     4   /' ',T34,'NUMBER = ',I5,//)
  115 FORMAT('0',T20,'Q(',I2,',',I2,')REAL = ',F10.5,/'0',
     1   T20,'Q(',I2,',',I2,')IMAG = ',F10.5,/)
  136 FORMAT('1')
      END
C                    THIS IS SUBROUTINE INPUT
C
      SUBROUTINE INPUT(IER)
C
C     SUBROUTINE INPUT READS INPUT VARIABLES, AND DEFINES
C     SEVERAL CONSTANTS USED THROUGHOUT THE PROGRAM.
C
      COMMON/BLCK1/ FSTRMN,DELTAS,DX,DH,DSTSTR,RO,RI,REDFRQ
      COMMON/BLCK2/ A1,A2,A3,A4,RN,RM,RM1,FACT1,FACT2
      COMMON/BLCK3/ NGRDFN,NPTS,LCOUNT,IHAVEP,N,M,M1,IPRINT
      NAMELIST/NAM1/ FSTRMN,REDFRQ,RO,RI,NGRDFN,N,M,M1,
     1   IPRINT
C
      WRITE(6,80)
      READ(5,NAM1)
      WRITE(6,NAM1)
C
      FMANGL = ARSIN(1./FSTRMN)
      DH = (RO - RI)/FLOAT(NGRDFN)
C
      IF ( DH .LT. 0. ) GO TO 1
C
      DELTAS = DH*FSTRMN
      DX = DH/TAN(FMANGL)
      DSTSTR = 2.*DX
      NPTS = 1./DSTSTR + 1
C
      IF ( NPTS .GT. 400 ) GO TO 2
C
      BETA = SQRT(FSTRMN*FSTRMN - 1.)
      RN = FLOAT(N)
      RM = FLOAT(M)
      RM1 = FLOAT(M1)
      FACT1 = REDFRQ*REDFRQ
      FACT2 = RN*RN/(FSTRMN*FSTRMN)
C
C     COMPUTE CONSTANTS TO BE USED IN THE COMPUTATIONAL
C     MOLECULES.
C
      A1 = 0.25*DELTAS/FSTRMN
      A2 = 0.5*FSTRMN/BETA
      A3 = REDFRQ*DELTAS*A2
      A4 = 0.5*FSTRMN
      RETURN
C
    1 IER = 1
      WRITE(6,100)
      GO TO 3
C
    2 IER = 1
      WRITE(6,110)
    3 RETURN
   80 FORMAT('1')
  100 FORMAT(//' ',35X,'ABNORMAL TERMINATION: INPUT RADII ',
     1   'INCORRECT',//)
  110 FORMAT(//' ',35X,'ABNORMAL TERMINATION: MUST INCREAS',
     1   'E THE SIZE OF VECTORS XPT, CPR, AND CPI',//)
      END
C                    THIS IS SUBROUTINE INITAL
C
      SUBROUTINE INITAL
C
C     SUBROUTINE INITAL INITIALIZES ALL FLOW FIELD
C     QUANTITIES.
C
      COMPLEX DPHIDR,DPHIDX
```

```
      COMPLEX PHI(400),DPHIS1(400),DPHIS2(400)
      DIMENSION X(400),R(400),XPT(400),CPR(400),CPI(400)
      COMMON/BLCK1/ FSTRMN,DELTAS,DX,DH,DSTSTR,RO,RI,REDFRQ
      COMMON/BLCK2/ A1,A2,A3,A4,RN,RM,RM1,FACT1,FACT2
      COMMON/BLCK3/ NGRDFN,NPTS,LCOUNT,IHAVEP,N,M,M1,IPRINT
      COMMON/BLCK4/ PHI,DPHIS1,DPHIS2
      COMMON/BLCK5/ X,R,XPT,CPR,CPI
      DATA PI/3.141593/
C
      X(1) = 0.
      R(1) = RO
      XPT(1) = 0.
C
C     ALONG THE INITIAL RIGHT RUNNING CHARACTERISTIC PHI AND
C     DPHIS2 ARE ZERO.
C
      PHI(1) = (0.,0.)
      DPHIS2(1) = (0.,0.)
C
C
      AA=.2/FSTRMN
      DPHIS1(1) = CMPLX(AA,0.)
      DPHIDR = A4*DPHIS1(1)
      DPHIDX = A2*DPHIS1(1)
      CPR(1) = -2.*REAL(DPHIDX)
      CPI(1) = -2.*AIMAG(DPHIDX)
C
      IF ( IPRINT .NE. 1 ) RETURN
      WRITE(6,90)
      WRITE(6,95)
      WRITE(6,100) X(1),DPHIS1(1),DPHIS2(1),PHI(1),
     1   R(1),DPHIDR,DPHIDX
      WRITE(6,110) CPR(1),CPI(1)
      RETURN
   90 FORMAT('1',T10,'X',T22,'D(PHI)/D(S1)',T46,
     1   'D(PHI)/D(S2)',T70,'PHI')
   95 FORMAT(' ',T10,'R',T23,'D(PHI)/DR',T47,'D(PHI)/DX',/)
  100 FORMAT(3H I ,2X,F8.4,4X,3(F12.5,F9.5,3X),/' ',4X,F8.4,
     1   4X,3(F12.5,F9.5,3X))
  110 FORMAT('0',10X,'INITIAL VALUE:  INNER SURFACE OF',
     1   ' OUTER CYLINDER',/' ',30X,'CP(REAL) = ',F8.4,10X,
     2   'CP(IMAG) = ',F8.4,//)
      END
C                  THIS IS SUBROUTINE COMPXR
C
      SUBROUTINE COMPXR
C
C     SUBROUTINE COMPXR COMPUTES THE (X,R) COORDINATES OF A
C     GRID POINT.
C
      DIMENSION X(400),R(400),XPT(400),CPR(400),CPI(400)
      COMMON/BLCK1/ FSTRMN,DELTAS,DX,DH,DSTSTR,RO,RI,REDFRQ
      COMMON/BLCK3/ NGRDFN,NPTS,LCOUNT,IHAVEP,N,M,M1,IPRINT
      COMMON/BLCK5/ X,R,XPT,CPR,CPI
C
      I = IHAVEP + 1
      J = IHAVEP
C
C     IF THIS IS THE FIRST POINT ON A NEW RIGHT RUNNING MACH
C     LINE, GO TO 1.
C
      IF ( J .EQ. 0 ) GO TO 1
C
      X(I) = X(J) + DX
      R(I) = R(J) -DH
      RETURN
C
    1 R(I) = RO
      X(1) = X(1) + DSTSTR
      RETURN
      END
C                  THIS IS SUBROUTINE MACHLN
```

```
C
      SUBROUTINE MACHLN
C
C     SUBROUTINE MACHLN COMPUTES THE VALUES OF THE FLOW
C     FIELD QUANTITIES ALONG THE INITIAL RIGHT-RUNNING MACH
C     LINE WHERE PHI AND DPHIS2 ARE ZERO.
C
      COMPLEX A,C
      COMPLEX DPHIDR,DPHIDX
      COMPLEX PHI(400),DPHIS1(400),DPHIS2(400)
      DIMENSION X(400),R(400),XPT(400),CPR(400),CPI(400)
      COMMON/BLCK1/ FSTRMN,DELTAS,DX,DH,DSTSTR,RO,RI,REDFRQ
      COMMON/BLCK2/ A1,A2,A3,A4,RN,RM,RM1,FACT1,FACT2
      COMMON/BLCK3/ NGRDFN,NPTS,LCOUNT,IHAVEP,N,M,M1,IPRINT
      COMMON/BLCK4/ PHI,DPHIS1,DPHIS2
      COMMON/BLCK5/ X,R,XPT,CPR,CPI
C
      I = IHAVEP + 1
      J = IHAVEP
C
C
C     CALCULATE THE COEFFICIENTS ASSOCIATED WITH THE RIGHT-
C     RUNNING MACH LINE.
C     LINE.
C
      AA1 = 1. - A1/R(I)
      A = CMPLX(AA1,A3)
      C1 = 1. + A1/R(J)
      C = DPHIS1(J)*CMPLX(C1,-A3)
C
      PHI(I) = (0.,0.)
      DPHIS2(I) = (0.,0.)
      DPHIS1(I) = C/A
C
      DPHIDR =  A4*DPHIS1(I)
      DPHIDX = A2*DPHIS1(I)
C
      IF ( IPRINT .NE. 1 ) RETURN
      WRITE(6,100) X(I),DPHIS1(I),DPHIS2(I),PHI(I),
     1   R(I),DPHIDR,DPHIDX
      WRITE(6,111)
      RETURN
  100 FORMAT(3H M ,2X,F8.4,4X,3(F12.5,F9.5,3X),/' ',4X,F8.4,
     1   4X,3(F12.5,F9.5,3X))
  111 FORMAT('0')
      END
C                   THIS IS SUBROUTINE RAD1
C
C     THIS IS SUBROUTINE RAD1
      SUBROUTINE RAD1
C
C     SUBROUTINE RAD1 COMPUTES THE FLOW FIELD QUANTITIES AT
C     THE SURFACE OF THE INNER RADIUS WHERE THE BOUNDARY
C     CONDITION IS  DEPENDENT ON N , THE CIRCUMFERENTIAL
C     MODE NUMBER.  IF  N  IS:
C        EVEN  --  DPHIDR = 0, AND THUS DPHIS1 = DPHIS2.
C        ODD   --  CP = 0.
C
      COMPLEX A,B,C,TANR,DPHIDR,DPHIDX,DELTA,GAMMA,IK
      COMPLEX PHI(400),DPHIS1(400),DPHIS2(400)
      DIMENSION X(400),R(400),XPT(400),CPR(400),CPI(400)
      COMMON/BLCK1/ FSTRMN,DELTAS,DX,DH,DSTSTR,RO,RI,REDFRC
      COMMON/BLCK2/ A1,A2,A3,A4,RN,RM,RM1,FACT1,FACT2
      COMMON/BLCK3/ NGRDFN,NPTS,LCOUNT,IHAVEP,N,M,M1,IPRINT
      COMMON/BLCK4/ PHI,DPHIS1,DPHIS2
      COMMON/BLCK5/ X,R,XPT,CPR,CPI
C
      I = IHAVEP + 1
      J = IHAVEP
C
C     CALCULATE THE COEFFICIENTS ASSOCIATED WITH THE RIGHT-
C     RUNNING MACH LINE.
C
```

```
C                                                                   C
C     THE FOLLOWING VARIABLE, IK, WAS FOUND TO BE                   C
C     UNDEFINED IN THE ORIGINAL REFERENCE 12 PROGRAM, AND           C
C     WAS THE REASON FOR A NUMERICAL INSTABILITY AFTER THE          C
C     FIRST REFLECTION.                                             C
C                                                                   C
      IK=CMPLX(0.0,REDFRQ)
      AA1 = 1. - A1/R(I)
      A = CMPLX(AA1,A3)
      B1 = A1/R(I) - 0.25*DELTAS*DELTAS*(FACT1 -
     1   FACT2/(R(I)*R(I)))
      B = CMPLX(B1,A3)
      C1 = 1. + A1/R(J)
      C2 = -A1/R(J) + 0.25*DELTAS*DELTAS*(FACT1 -
     1   FACT2/(R(I)*R(I)))
      C3 = (2.*FACT1 - FACT2/(R(J)*R(J)) -
     1   FACT2/(R(I)*R(I)))*DELTAS*0.5
      C = DPHIS1(J)*CMPLX(C1,-A3) + DPHIS2(J)*CMPLX(C2,-A3)
     1   + PHI(J)*CMPLX(C3,0.)
C
      IF ( MOD(N,2) .EQ. 0 ) GO TO 1
C
C     APPLY THE BOUNDARY CONDITION FOR ODD VALUES OF N.
C     CP = (IK)PHI + DPHIDX = 0.  USE THIS B.C., THE FINITE
C     DIFFERENCE EQN. FOR DPHIDX, AND THE EQN. FOR THE RIGHT
C     RUNNING MACHLINE TO SOLVE FOR DPHIS1 AND DPHIS2.
C
      DELTA = A2 + 0.5*IK*DELTAS
      GAMMA = IK*( PHI(J) + 0.5*DELTAS*DPHIS2(J) )
C
C     SOLVING FOR DPHIS1 AND DPHIS2
C
      DPHIS1(I) = ( C + B*GAMMA/DELTA )/( A - B*A2/DELTA )
      DPHIS2(I) = ( C - A*DPHIS1(I) )/B
C
      DPHIDX = A2*( DPHIS1(I) + DPHIS2(I) )
      DPHIDR = A4*( DPHIS1(I) - DPHIS2(I) )
      GO TO 2
C
C     APPLY THE BOUNDARY CONDITION FOR EVEN VALUES OF  N.
C
    1 DPHIS1(I) = C/(A+B)
      DPHIS2(I) = DPHIS1(I)
      DPHIDR = (0.,0.)
      DPHIDX = A2*(DPHIS1(I) + DPHIS2(I))
C
C     PHI.
C
    2 PHI(I) = PHI(J) + 0.5*(DPHIS2(J) + DPHIS2(I))*DELTAS
C
      IF ( IPRINT .NE. 1 ) RETURN
      WRITE(6,100) X(I),DPHIS1(I),DPHIS2(I),PHI(I),
     1   R(I),DPHIDR,DPHIDX
      RETURN
  100 FORMAT(3H RI,2X,F8.4,4X,3(F12.5,F9.5,3X),/' ',4X,F8.4,
     1   4X,3(F12.5,F9.5,3X))
      END
C                   THIS IS SUBROUTINE RAD2
C
      SUBROUTINE RAD2
C
C     SUBROUTINE RAD2 COMPUTES THE FLOW FIELD QUANTITIES AT
C     THE INNER SURFACE OF THE OUTER CYLINDER, WHERE THE
C     FLOW TANGENCY CONDITION PRESCRIBES DPHIDR.
C
      COMPLEX D,E,F,TANR
      COMPLEX DPHIDR,DPHIDX
      COMPLEX PHI(400),DPHIS1(400),DPHIS2(400)
      DIMENSION X(400),R(400),XPT(400),CPR(400),CPI(400)
      COMMON/BLCK1/ FSTRMN,DELTAS,DX,DH,DSTSTR,RO,RI,REDFRQ
      COMMON/BLCK2/ A1,A2,A3,A4,RN,RM,RM1,FACT1,FACT2
      COMMON/BLCK3/ NGRDFN,NPTS,LCOUNT,IHAVEP,N,M,M1,IPRINT
```

```
      COMMON/BLCK4/ PHI,DPHIS1,DPHIS2
      COMMON/BLCK5/ X,R,XPT,CPR,CPI
      DATA PI/3.141593/
C
      I = IHAVEP + 1
      J = IHAVEP + 2
      K = LCOUNT
      ARG=RM*PI*X(I)
C
C
C     CALCULATE THE COEFFICIENTS ASSOCIATED WITH THE LEFT
C     RUNNING MACH LINE.
C
      D1 = A1/R(I) + 0.25*DELTAS*DELTAS*(FACT1 - FACT2/(R(I)
     1   *R(I)))
      D = CMPLX(D1,-A3)
      E1 = -1. - A1/R(I)
      E = CMPLX(E1,-A3)
      F1 = -A1/R(J) - 0.25*DELTAS*DELTAS*(FACT1 - FACT2/
     1   (R(I)*R(I)))
      F2 = -1. + A1/R(J)
      F3 = (2.*FACT1 - FACT2/(R(I)*R(I)) - FACT2/(R(J)*
     1   R(J)))*DELTAS*0.5
      F = DPHIS1(J)*CMPLX(F1,A3) + DPHIS2(J)*CMPLX(F2,A3) -
     1   PHI(J)*CMPLX(F3,0.)
C
C     CALCULATE THE FLOW TANGENCY CONDITION  -  TANR
C
C     BOUNDARY CONDITIONS FOR PANEL FLUTTER
C
C                                                                      C
C     THE FOLLOWING THREE CARDS WERE MODIFIED FROM THE                 C
C     ORIGINAL REFERENCE 12 PROGRAM.                                   C
C                                                                      C
      ALPHA=.1
      TANR1=ALPHA
      TANR2=REDFRQ*X(I)*ALPHA
      TANR = CMPLX(TANR1,TANR2)
C
      DPHIS1(I) = ( F + TANR*E/A4 )/( D + E )
      DPHIS2(I) = ( F - TANR*D/A4 )/( D + E )
      DPHIDR = A4*(DPHIS1(I) - DPHIS2(I))
      DPHIDX = A2*(DPHIS1(I) + DPHIS2(I))
C
C     INTEGRATE ALONG THE LEFT RUNNING MACH LINE TO FIND PHI
C
      PHI(I) = PHI(J) + 0.5*(DPHIS1(J) + DPHIS1(I))*DELTAS
C
C     CALCULATE THE PRESSURE COEFFICIENT AT THIS GRID POINT.
C
      XPT(K) = X(I)
      CPR(K) = -2.*(-REDFRQ*AIMAG(PHI(I)) + REAL(DPHIDX))
      CPI(K) = -2.*(REDFRQ*REAL(PHI(I)) + AIMAG(DPHIDX))
C
      IF ( IPRINT .NE. 1 ) RETURN
      WRITE(6,100) X(I),DPHIS1(I),DPHIS2(I),PHI(I),
     1   R(I),DPHIDR,DPHIDX,TANR
      WRITE(6,110) CPR(K),CPI(K)
      RETURN
  100 FORMAT(3H RO,2X,F8.4,4X,3(F12.5,F9.5,3X),/' ',4X,F8.4,
     1   4X,3(F12.5,F9.5,3X))
  110 FORMAT('0',10X,'INNER SURFACE OF OUTER CYLINDER',/' ',
     1   30X,'CP(REAL) = ',F8.4,10X,'CP(IMAG) = ',F8.4,//)
      END
C                THIS IS SUBROUTINE GENFPT
C
      SUBROUTINE GENFPT(IER)
C
C     SUBROUTINE GENFPT COMPUTES THE FLOW FIELD QUANTITIES
C     AT A GENERAL FLOW FIELD POINT.
C
      COMPLEX PHIL
```

```
      CCMPLEX A,B,C,D,E,F,DENOM
      CCMPLEX DPHIDR,DPHIDX
      CCMPLEX PHI(400),DPHIS1(400),DPHIS2(400)
      DIMENSION X(400),R(400),XPT(400),CPR(400),CPI(400)
      CCMMON/BLCK1/ FSTRMN,DELTAS,DX,DH,DSTSTR,RO,RI,REDFRC
      COMMON/BLCK2/ A1,A2,A3,A4,RN,RM,RM1,FACT1,FACT2
      CCMMON/BLCK3/ NGRDFN,NPTS,LCOUNT,IHAVEP,N,M,M1,IPRINT
      CCMMCN/BLCK4/ PHI,DPHIS1,DPHIS2
      COMMON/BLCK5/ X,R,XPT,CPR,CPI
C
      I = IHAVEP + 1
      J = IHAVEP
      K = IHAVEP + 2
C
C     CCMPUTE THE COEFFICIENTS OF DPHIS1 AND DPHIS2.
      FACT3 = FACT2/(R(I)*R(I))
      FACT4 = FACT2/(R(K)*R(K))
      FACT5 = FACT2/(R(J)*R(J))
C
C     A,B AND C ARE ASSOCIATED WITH THE RIGHT RUNNING MACH
C     LINE, WHILE D,E AND F ARE ASSOCIATED WITH THE LEFT.
C
      AA1 = 1. - A1/R(I)
      A = CMPLX(AA1,A3)
      B1 = -AA1 + 1. - 0.25*DELTAS*DELTAS*(FACT1 - FACT3)
      B = CMPLX(B1,A3)
      C1 = 1. + A1/R(J)
      C2 = -C1 + 1. + 0.25*DELTAS*DELTAS*(FACT1 - FACT3)
      C3 = (2.*FACT1 - FACT3 - FACT5)*DELTAS*0.5
      C = DPHIS1(J)*CMPLX(C1,-A3) + DPHIS2(J)*CMPLX(C2,-A3)
     1    + PHI(J)*CMPLX(C3,0.)
C
      D1 = A1/R(I) + 0.25*DELTAS*DELTAS*(FACT1 - FACT3)
      D = CMPLX(D1,-A3)
      E1 = -1. - A1/R(I)
      E = CMPLX(E1,-A3)
      F1 = -A1/R(K) - 0.25*DELTAS*DELTAS*(FACT1 - FACT3)
      F2 = -1. + A1/R(K)
      F3 = (2.*FACT1 - FACT3 - FACT4)*DELTAS*0.5
      F = DPHIS1(K)*CMPLX(F1,A3) + DPHIS2(K)*CMPLX(F2,A3) -
     1    PHI(K)*CMPLX(F3,0.)
C
C     USE CRAMERS RULE TO SOLVE FCR DPHIS1 AND DPHIS2
C     PRCVIDED THAT THE DETERMINANT OF COEFFICIENTS IS NCN-
C     SINGULAR.
C
      DENCM = A*E - D*B
      IF ( CABS( DENOM ) .LT. 1.E-05 ) GO TO 1
      DPHIS1(I) = (C*E - B*F)/DENOM
      DPHIS2(I) = (A*F - C*D )/DENOM
      DPHIDR = A4*(DPHIS1(I) - DPHIS2(I))
      DPHIDX = A2*(DPHIS1(I) + DPHIS2(I))
C
C     INTEGRATE ALONG THE RIGHT RUNNING MACH LINE TO FIND
C     PHI.
C
      PHI(I) = PHI(J) + 0.5*(DPHIS2(I) + DPHIS2(J))*DELTAS
      PHIL = PHI(K) + 0.5*(DPHIS1(K) + DPHIS1(I))*DELTAS
C
      IF ( IPRINT .NE. 1 ) RETURN
      WRITE(6,100) X(I),DPHIS1(I),DPHIS2(I),PHI(I),
     1    R(I),DPHIDR,DPHIDX, PHIL
      WRITE(6,111)
      RETURN
C
    1 IER = 1
      WRITE(6,110) DENOM
      RETURN
  100 FORMAT(3H G ,2X,F8.4,4X,3(F12.5,F9.5,3X),/' ',4X,F8.4,
     1    4X,3(F12.5,F9.5,3X))
  110 FORMAT('0',///,' ',35X,'ABNORMAL TERMINATION: ',
     1    'DETERMINANT OF COEFFICIENTS IS SINGULAR',/'0',50X,
```

```
     2    'DENOMINATOR = ',E12.5)
  111 FORMAT('0')
      END
C                    THIS IS SUBROUTINE QSF
C        SUBROUTINE QSF
      SUBROUTINE QSF(H,Y,Z,NDIM)
C            CALL QSF (H,Y,Z,NDIM)
C        DESCRIPTION OF PARAMETERS
C            H       - THE INCREMENT OF ARGUMENT VALUES.
C            Y       - THE INPUT VECTOR OF FUNCTION VALUES.
C            Z       - THE RESULTING VECTOR OF INTEGRAL
C                      VALUES.  Z  MAY BE IDENTICAL WITH  Y.
C                      IDENTICAL WITH Y.
C            NDIM    - THE DIMENSION OF VECTORS Y AND Z.
C
C        REMARKS
C            NO ACTION IN CASE NDIM LESS THAN 3.
C
C
C
      DIMENSION Y(1),Z(1)
C
      HT=.3333333*H
      IF(NDIM-5)7,8,1
C
C     NDIM IS GREATER THAN 5. PREPARATIONS OF INTEGRATION
C     LOOP
C
    1 SUM1=Y(2)+Y(2)
      SUM1=SUM1+SUM1
      SUM1=HT*(Y(1)+SUM1+Y(3))
      AUX1=Y(4)+Y(4)
      AUX1=AUX1+AUX1
      AUX1=SUM1+HT*(Y(3)+AUX1+Y(5))
      AUX2=HT*(Y(1)+3.875*(Y(2)+Y(5))+2.625*(Y(3)+Y(4))+
     1    Y(6))
      SUM2=Y(5)+Y(5)
      SUM2=SUM2+SUM2
      SUM2=AUX2-HT*(Y(4)+SUM2+Y(6))
      Z(1)=0.
      AUX=Y(3)+Y(3)
      AUX=AUX+AUX
      Z(2)=SUM2-HT*(Y(2)+AUX+Y(4))
      Z(3)=SUM1
      Z(4)=SUM2
      IF(NDIM-6)5,5,2
C
C     INTEGRATION LOOP
    2 DO 4 I=7,NDIM,2
      SUM1=AUX1
      SUM2=AUX2
      AUX1=Y(I-1)+Y(I-1)
      AUX1=AUX1+AUX1
      AUX1=SUM1+HT*(Y(I-2)+AUX1+Y(I))
      Z(I-2)=SUM1
      IF(I-NDIM)3,6,6
    3 AUX2=Y(I)+Y(I)
      AUX2=AUX2+AUX2
      AUX2=SUM2+HT*(Y(I-1)+AUX2+Y(I+1))
    4 Z(I-1)=SUM2
    5 Z(NDIM-1)=AUX1
      Z(NDIM)=AUX2
      RETURN
    6 Z(NDIM-1)=SUM2
      Z(NDIM)=AUX1
      RETURN
C     END OF INTEGRATION LOOP
C
    7 IF(NDIM-3)12,11,8
C
C     NDIM IS EQUAL TO 4 OR 5
    8 SUM2=1.125*HT*(Y(1)+Y(2)+Y(2)+Y(2)+Y(3)+Y(3)+Y(3)+
```

```
     1   Y(4))
      SUM1=Y(2)+Y(2)
      SUM1=SUM1+SUM1
      SUM1=HT*(Y(1)+SUM1+Y(3))
      Z(1)=0.
      AUX1=Y(3)+Y(3)
      AUX1=AUX1+AUX1
      Z(2)=SUM2-HT*(Y(2)+AUX1+Y(4))
      IF(NDIM-5)10,9,9
    9 AUX1=Y(4)+Y(4)
      AUX1=AUX1+AUX1
      Z(5)=SUM1+HT*(Y(3)+AUX1+Y(5))
   10 Z(3)=SUM1
      Z(4)=SUM2
      RETURN
C
C     NDIM IS EQUAL TO 3
   11 SUM1=HT*(1.25*Y(1)+Y(2)+Y(2)-.25*Y(3))
      SUM2=Y(2)+Y(2)
      SUM2=SUM2+SUM2
      Z(3)=HT*(Y(1)+SUM2+Y(3))
      Z(1)=0.
      Z(2)=SUM1
   12 RETURN
      END
```

The outer flowfield program, from reference 13, consists of 5 subroutines and a main program to manipulate the subroutines. The action of each particular subroutine is indicated in the program listing. Inputs required to the program must be on two cards, and are as follows:

DATE

MACH Mach number.

RADIUS Radius to length ratio.

K Reduced frequency.

MFREQ Axial mode number.

NR The r in Qmr, the generalized aerodynamic force.

NFREQ Circumferential mode number.

FINGRD Grid fineness, essentially the number of grid points along the cylinder surface.

The run date is typed onto the first card. The second card contains the above parameters in the following format: F20.8, 2F10.3, 4I5. Of the above parameters, in the modified program, MFREQ, NR, and NFREQ must be set to 1, as the case under consideration is not panel flutter but a cylinder at angle of attack. Other parameters are arbitrary.

```
C
C           LINEARIZED METHOD OF CHARACTERISTICS
C     FOR   SUPERSONIC FLOW PAST A VIBRATING CYLINDRICAL SHELL
C
      DIMENSION DATE(3)
      DIMENSION XN(400)
      COMMON DPHII,DPHIK,PHI(400,2),PHK(400,2),QPHI(400,2),IPHI1,IPHI2,
     4IKM,IKW,PARW,W,II,REALCP(400),CP(400),AMAGCP(400),
     1    MACH,K,MANGL,RADIUS,DELTAS,XLENGT,BETA,DSTSTR,HDSTRL,TRNGLH,
     2 X(400,2),R(400,2),NFREQ,FINGRD,ISWTCH,JSWTCH,ILINE,MLINE,JLINE,
     3 MFREQ,IHAVEP,KOUNT
      INTEGER FINGRD
      REAL   MACH,MANGL,K
      COMPLEX DPHII,DPHIK,PHI,IKM,CP,PX ,IPHI1,IPHI2,IKW,PHK,II,QPHI,PR
C
C     PRINT NAME OF PROGRAM AND DATE OF RUN
C
      READ (5,10)DATE
 10   FORMAT (3A4)
  11  FORMAT ('1',/////,40X,'LINEARIZED METHOD OF CHARACTERISTICS'//40X,
     1'FOR SUPERSONIC FLOW PAST A VIBRATING CYLINDRICAL SHELL'//20X
     2'DATE OF RUN-',3A4///)
      WRITE (6,11) DATE
C
C     READ INPUT
C
      READ(5,1)MACH,RADIUS,K,MFREQ,NR,NFREQ,FINGRD
    1 FORMAT(F20.8,2F10.3,4I5)
C
C     COMPUTE CONSTANTS
C
      II=(0.0,1.0)
      BETA=SQRT(MACH**2-1.0)
      MANGL=ARSIN(1.0/MACH)
      XLENGT=1./(2.*COS(MANGL))
      HEIGHT=SIN(MANGL)*XLENGT
      DELTAS=XLENGT /FINGRD
      DSTSTR=DELTAS*COS(MANGL)*2.0
      HDSTRL=.5*DSTSTR
      ML=IFIX(FINGRD+1.0)
      TRNGLH=HDSTRL*TAN(MANGL)
C
C     SET COUNTERS
C
 20   ISWTCH=2
      JSWTCH=1
      IHAVEP=1
      KOUNT=1
```

```
C                                                                       00000480
C     COMPUTE INTIAL VALUES                                             00000490
C                                                                       00000500
      I=IHAVEP                                                          00000510
      QPHI(I,JSWTCH)=(0.,0.)                                            00000520
      PHK(I,JSWTCH)=(0.,0.)                                             00000530
      X(IHAVEP,JSWTCH)=0.0                                              00000540
      R(IHAVEP,JSWTCH)=RADIUS                                           00000550
      PI=3.141593                                                       00000560
C                                                             C
C     THE FOLLOWING CARD WAS MODIFIED FROM THE ORIGINAL       C
C     REFERENCE 13 PROGRAM.                                   C
C                                                             C
      PARW=.1
      QR=PARW                                                           00000580
      PHI(I,JSWTCH)=-2.0*QR/MACH                                        00000590
      PX=(MACH/(2.0*BETA))*(PHK(I,JSWTCH)+PHI(I,JSWTCH))                00000600
      CP(KOUNT)=-2.0*(II*K*QPHI(I,JSWTCH)+PX)                           00000610
      REALCP(KOUNT)=REAL(CP(KOUNT))                                     00000620
      AMAGCP(KOUNT)=AIMAG(CP(KOUNT))                                    00000630
C                                                                       00000640
C     WRITE OUT INPUT                                                   00000650
C                                                                       00000660
      WRITE (6,12) MACH,K,NFREQ,FINGRD ,RADIUS ,MFREQ                   00000670
 12   FORMAT (1HO,20X,'FREESTREAM MACH NUMBER =',F9.6//20X,'REDUCED FREQ00000680
     1=',F9.5//20X,'RAD MODE NO. N   =',I2//20X,'GRID FINENESS IS = ',  00000690
     2 I3  //20X,'CYLINDER RADIUS IS =',F9.2//20X,'AXIAL MODE NO. M   ='00000700
     3,I2)                                                              00000710
      KOUNT=2                                                           00000720
C                                                                       00000730
C     COMPXR COMPUTES THE VALUE FOR X AND R GIVEN IHAVEP,ISWTCH         00000740
C                                                                       00000750
 104   CALL COMPXR                                                      00000760
C                                                             C
C     THE FOLLOWING TWO CARDS WERE MODIFIED FROM THE          C
C     ORIGINAL REFERENCE 13 PROGRAM.                          C
C                                                             C
      PARW=.1
      W=.1*X(IHAVEP,ISWTCH)
      XKM=(K*MACH)/BETA                                                 00000790
      IKM=II*XKM                                                        00000800
      XKW=K*W                                                           00000810
      IKW=II*XKW                                                        00000820
C                                                                       00000830
C     THE PROGRAM NOW GOES TO 30 IF POINT IS ON INITIAL MACH LINE.      00000840
C                                                                       00000850
 1001  IF (IHAVEP.EQ.1) GO TO 30                                        00000860
C                                                                       00000870
```

```
C     TEST WHETHER THIS IS A SURFACE POINT.
C
      IF  (IHAVEP.EQ.KOUNT) GO TO 40
      GO TO 60
C
 30    CALL MACHLN
      GO TO 50
C
 40   CALL PANPNT
      GO TO 50
C
 60   CALL GENFPT
   50 A=IHAVEP
      B=ISWTCH
      PX=(MACH/(2.0*BETA))*(PHK(A,B)+ PHI(A,B))
      PR=(MACH/2.0)*(PHK(A,B)-PHI(A,B))
 1000   IF (IHAVEP.EQ.KOUNT) GO TO 25
      GC TO 35
C
C     INCREMENT FOR NEXT LINES
C
 25   IF (ISWTCH.EQ.1.) GO TO 103
      ISWTCH=1
      JSWTCH=2
      IHAVEP=1
      GO TO 108
 103  ISWTCH=2
      JSWTCH=1
      IHAVEP=1
      GO TO 108
C
C     AT 35 INCREMENT ALONG PRESENT LINE
C
 35   IHAVEP=IHAVEP+1
      GO TO 104
 108   KOUNT=KOUNT+1
      IF ((KOUNT-1).EQ.ML)GO TO 101
      GO TO 104
  101 CONTINUE
      CALL  INTEG(REALCP,MFREQ,NR,DSTSTR,ML)
      CALL  INTEG(AMAGCP,MFREQ,NR,DSTSTR,ML)
C                                                                   C
C     THE FOLLOWING CARDS WERE MODIFIED FROM THE ORIGINAL           C
C     REFERENCE 13 PROGRAM TO ENABLE GRAPHICAL CP OUTPUT.           C
C                                                                   C
      XN(1)=0.0
      DO 115 I=1,ML
      XN(I+1)=XN(I)+1./ML
```

```
  115 CONTINUE
      WRITE(6,998)
  998 FORMAT('1','CP REAL')
      CALL PLOTP(XN,REALCP,ML,0)
      WRITE(6,999)
  999 FORMAT('1','CP IMAGINARY')
      CALL PLOTP(XN,AMAGCP,ML,0)
      STOP
      END
C
      SUBROUTINE COMPXR
C
      REAL    MACH,MANGL,K,KW
C
C     CCMPUTES THE X AND R COORDINATES
C
      CCMMON DPHII,DPHIK,PHI(400,2),PHK(400,2),QPHI(400,2),IPHI1,IPHI2,
     4IKM,IKW,PARW,W,II,REALCP(400),CP(400),AMAGCP(400),
     1    MACH,K,MANGL,RADIUS,DELTAS,XLENGT,BETA,DSTSTR,HDSTRL,TRNGLH,
     2  X(400,2),R(400,2),NFREQ,FINGRD,ISWTCH,JSWTCH,ILINE,MLINE,JLINE,
     3  MFREQ,IHAVEP,KOUNT
      COMPLEX DPHII,DPHIK,PHI,IKM,CP,PX ,IPHI1,IPHI2,IKW,PHK,II,QPHI,PR
      INTEGER FINGRD
C
C     TEST FCR POINT ON MACH LINE
C
      IF (IHAVEP.EQ.1) GO TO 10
      I=IHAVEP
      J=IHAVEP-1
      X(I,ISWTCH)=X(J     ,ISWTCH)+HDSTRL
      R(I,ISWTCH)=R(J     ,ISWTCH)      -TRNGLH
      RETURN
   10 I=IHAVEP
      X(I,ISWTCH)=X(I     ,JSWTCH)+HDSTRL
      P(I,ISWTCH)=R(I     ,JSWTCH)+TRNGLH
      RETURN
      END
      SUBROUTINE MACHLN
      CCMMON DPHII,DPHIK,PHI(400,2),PHK(400,2),QPHI(400,2),IPHI1,IPHI2,
     4IKM,IKW,PARW,W,II,REALCP(400),CP(400),AMAGCP(400),
     1    MACH,K,MANGL,RADIUS,DELTAS,XLENGT,BETA,DSTSTR,HDSTRL,TRNGLH,
     2  X(400,2),P(400,2),NFREQ,FINGRD,ISWTCH,JSWTCH,ILINE,MLINE,JLINE,
     3  MFREQ,IHAVEP,KOUNT
      REAL    MACH,MANGL,K,KW
      COMPLEX             AA2,
     1A,B,C,D,DPHII,DPHIK,PHI,IKM,CP,PX ,IPHI1,IPHI2,IKW,PHK,II,QPHI
     2 ,PR
      INTEGER FINGRD
```

```
      I=IHAVEP                                                          00001690
      PHK(I,ISWTCH)=(0.,0.)                                             00001700
      A=1.+DELTAS/(4.*R(I,ISWTCH)*MACH)+0.5*IKM*DELTAS                  00001710
      AA2=1.-DELTAS/ (4.*R(I,JSWTCH)*MACH)-0.5*IKM*DELTAS               00001720
      PHI(I,ISWTCH)=PHI(I,JSWTCH)*(AA2/A)                               00001730
      QPHI(I,ISWTCH)=(0.,0.)                                            00001740
10    RETURN                                                            00001750
      END                                                               00001760
      SUBROUTINE GENFPT                                                 00001770
C                                                                       00001780
C     GENFPT COMPUTES THE VELOCITY POTENTIAL AND ITS DERIVATIVES AT A   00001790
C     GENERAL FLOW FIELD POINT.                                         00001800
C                                                                       00001810
      COMMON DPHII,DPHIK,PHI(400,2),PHK(400,2),QPHI(400,2),IPHI1,IPHI2, 00001820
     4IKM,IKW,PARW,W,II,REALCP(400),CP(400),AMAGCP(400),                00001830
     1    MACH,K,MANGL,RADIUS,DELTAS,XLENGT,BETA,DSTSTR,HDSTRL,TRNGLH,  00001840
     2  X(400,2),R(400,2),NFREQ,FINGPD,ISWTCH,JSWTCH,ILINE,MLINE,JLINE, 00001850
     3  MFREQ,IHAVEP,KOUNT                                              00001860
      REAL    MACH,MANGL,K,KW,N                                         00001870
      COMPLEX                 AA1,AA2,AA3,                              00001880
     1A,B,C,D,DPHII,DPHIK,PHI,IKM,CP,PX ,IPHI1,IPHI2,IKW,PHK,II,QPHI    00001890
     2 ,PR,E,F                                                          00001900
      INTEGER FINGRD                                                    00001910
C                                                                       00001920
      I=IHAVEP                                                          00001930
      J=IHAVEP -1                                                       00001940
      N=FLOAT(NFREQ)                                                    00001950
C                                                                       00001960
      A=1.-DELTAS/(4.*R(I,ISWTCH)*MACH)+0.5*IKM*DELTAS                  00001970
C                                                                       00001980
      AA1=1.+DELTAS/(4.*R(J,ISWTCH)*MACH)-0.5*IKM*DELTAS                00001990
C                                                                       00002000
      AA3=-1.+DELTAS/ (4.*R(I,JSWTCH)*MACH)+0.5*IKM*DELTAS              00002010
C                                                                       00002020
      B=DELTAS/(4.*R(I,ISWTCH)*MACH)+0.5*IKM*DELTAS-0.25*DELTAS**2*     00002030
     1 (K**2-(N**2/(R(I,ISWTCH)**2*MACH**2)))                           00002040
C                                                                       00002050
C                                                                       00002060
      C=PHK(J,ISWTCH)*AA1+PHI(J,ISWTCH)*(-DELTAS/(4.*R(J,ISWTCH)*MACH)  00002070
     1 -0.5*IKM*DELTAS+0.25*DELTAS**2*(K**2-(N**2/(R(I,ISWTCH)**2*MACH**00002080
     22))))+ QPHI(J,ISWTCH)*DELTAS*0.5*(K**2- N**2/(R(J,ISWTCH)**2*MACH 00002090
     3**2))+    QPHI(J,ISWTCH)*DELTAS*0.5*(K**2- N**2/(R(I,ISWTCH)**2*  00002100
     4 MACH**2))                                                        00002110
C                                                                       00002120
C                                                                       00002130
      D=DELTAS/(4.0  *R(I,ISWTCH)*MACH)-0.5  *IKM*DELTAS+0.25  *DELTAS**00002140
     12*(K**2-(N**2/(R(I,ISWTCH)**2*MACH**2)))                          00002150
C                                                                       00002160
```

```
C                                                                       00002170
      F=PHI(I,JSWTCH)*AA3+PHK(I,JSWTCH)*(-DELTAS/(4.*R(I,JSWTCH)*MACH)  00002180
     1 +0.5*IKM*DELTAS-0.25*DELTAS**2*(K**2-(N**2/(R(I,ISWTCH)**2*MACH**00002190
     22))))- QPHI(I,JSWTCH)*DELTAS*0.5*(K**2- N**2/(R(I,JSWTCH)**2*MACH 00002200
     3**2))-    QPHI(I,JSWTCH)*DELTAS*0.5*(K**2- N**2/(R(I,ISWTCH)**2*  00002210
     4 MACH**2))                                                        00002220
C                                                                       00002230
      E=-1.-DELTAS/(4.*R(I,ISWTCH)*MACH)-0.5*IKM*DELTAS                 00002240
C                                                                       00002250
C     CRAMER'S RULE                                                     00002260
C                                                                       00002270
      PHK(I,ISWTCH)=(C*E-B*F)/(A*E -B*D)                                00002280
      PHI(I,ISWTCH)=(F*A-C*D)/(A*E -B*D)                                00002290
C                                                                       00002300
C     TRAPAZOIDAL RULE TO INTEGRATE.                                    00002310
C                                                                       00002320
      IPHI1=QPHI(I,JSWTCH)+0.5*(PHK(I,JSWTCH)+PHK(I,ISWTCH))*DELTAS     00002330
      IPHI2=QPHI(J,ISWTCH)+0.5*(PHI(J,ISWTCH)+PHI(I,ISWTCH))*DELTAS     00002340
C                                                                       00002350
C     AVERAGE THE TWO                                                   00002360
C                                                                       00002370
      QPHI(I,ISWTCH)=0.5*(IPHI1+IPHI2)                                  00002380
 15   RETURN                                                            00002390
      END                                                               00002400
      SUBROUTINE PANPNT                                                 00002410
C                                                                       00002420
C     PANPNT COMPUTES THE VALUES OF PHI'S AND QHPI AT A SURFACE POINT   00002430
C                                                                       00002440
      CCMMON DPHII,DPHIK,PHI(400,2),PHK(400,2),QPHI(400,2),IPHI1,IPHI2, 00002450
     4IKM,IKW,PARW,W,II,REALCP(400),CP(400),AMAGCP(400),                00002460
     1    MACH,K,MANGL,RADIUS,DELTAS,XLENGT,BETA,DSTSTR,HDSTRL,TRNGLH,  00002470
     2  X(400,2),R(400,2),NFREQ,FINGRD,ISWTCH,JSWTCH,ILINE,MLINE,JLINE, 00002480
     3  MFREQ,IHAVEP,KOUNT                                              00002490
      REAL   MACH,MANGL,K,KW,N                                          00002500
      COMPLEX                     AA1,AA2                               00002510
     1A,B,C,D,DPHII,DPHIK,PHI,IKM,CP,PX ,IPHI1,IPHI2,IKW,PHK,II,QPHI    00002520
     2 ,PR                                                              00002530
      INTEGER FINGRD                                                    00002540
      N=FLOAT(NFREQ)                                                    00002550
      I=IHAVEP                                                          00002560
      J=IHAVEP-1                                                        00002570
      A=1.-DELTAS/(4.*R(I,ISWTCH)*MACH)+0.5*IKM*DELTAS                  00002580
      AA1=1.+DELTAS/(4.*R(J,ISWTCH)*MACH)-0.5*IKM*DELTAS                00002590
      B=DELTAS/(4.*R(I,ISWTCH)*MACH)+0.5*IKM*DELTAS-0.25*DELTAS**2*     00002600
     1  (K**2-(N**2/(R(I,ISWTCH)**2*MACH**2)))                          00002610
      C=PHK(J,ISWTCH)*AA1+PHI(J,ISWTCH)*(-DELTAS/(4.*R(J,ISWTCH)*MACH)  00002620
     1 -0.5*IKM*DELTAS+0.25*DELTAS**2*(K**2-(N**2/(R(I,ISWTCH)**2*MACH**00002630
     22))))+ QPHI(J,ISWTCH)*DELTAS*0.5*(K**2- N**2/(R(J,ISWTCH)**2*MACH 00002640
```

```
     3**2))+    QPHI(J,ISWTCH)*DELTAS*0.5*(K**2- N**2/(R(I,ISWTCH)**2*
     4 MACH**2))
C
C
      PHK(I,ISWTCH)=       (C+B*(2.0/MACH)*(PARW+IKW))/(A+B)
      PHI(I,ISWTCH)=       (-A*(2.0/MACH)*(PARW+IKW)+C)/(A+B)
C
      QPHI(I     ,ISWTCH)=QPHI(J,ISWTCH)+0.5*(PHI(J,ISWTCH)+PHI(I     ,
     1  ISWTCH))*DELTAS
      PX=(MACH/(2.0*BETA))*(PHK(I,ISWTCH)+PHI(I,ISWTCH))
      CP(KOUNT)=-2.0*(II*K*QPHI(I,ISWTCH)+PX)
      REALCP(KOUNT)=REAL(CP(KOUNT))
      AMAGCP(KOUNT)=AIMAG(CP(KOUNT))
   10 RETURN
      END
      SUBROUTINE INTEG(Y,M,NR,DX,ML)
      DIMENSION Y(ML)
      Q=0.0
      X1=0.0
      RN=FLOAT(NR)
      PSI1=0.0
      PROD1=0.0
      DO 1 I=2,ML
      X2=X1+DX
      PSI2=.1*X2
      PROD2=PSI2*Y(I)
      Q=Q+(PROD2+PROD1)*DX/2.0
      PROD1=PROD2
      X1=X2
    1 CONTINUE
      Q=Q/2.0
      WRITE(6,100)M,NR,Q
  100 FORMAT(' ',10X,'Q(',I2,',',I2,')R=',E13.7,///)
  101 FORMAT('0','GENERALIZED AERODYNAMIC FORCE:',/)
      RETURN
      END
```

LIST OF REFERENCES

1. Grumman Research Dept., Rept. no. Re-488, *Self Excited Super Turbulence-The Whistler Nozzle*, Hill and Greene, October 1974.

2. Grumman Research Dept., *Effects of Initial Conditions on Mixing Rates of Turbulent Jets*, Hill and Jenkins, To Be Published.

3. Rockwell International, NR75H-129, *A Study of Potential Techniques for Increasing Jet Entrainment Rates In Ejector Augmenters*, Schum,E.F., October 1974.

4. ARL 75-0224, *Thrust Augmenting Ejectors*, Viets, H., June 1975.

5. Crow and Champagne, "Orderly Structure in Jet Turbulence", *Jo. of Fluid Mechanics*, Vol 48, 1971.

6. Bevilaqua and Lykoudis, "The Mechanism of Entrainment", *AIAA Jo.*, Volume 9, August, 1971.

7. Ricou and Spalding, "Measurement of Entrainment by Axisymmetric Turbulent Jets", *Jo. of Fluid Mechanics*, Volume 11, 1971.

8. AFFDL-TR-73-55, *Advanced Ejector Thrust Augmentation Study-Mass Entrainment Of Axisymmetric And Rectangular Free Jets*, Peschke, W., April 1973.

9. AEDC-TR-71-36, *Free Turbulent Mixing: A Critical Evaluation Of Theory And Experiment*, Harsha, P.T. ,February 1971.

10. Weinger, S.D., "The Effects of Sound on a Reattaching

Jet at Low Reynolds Numbers", *Fluid Amplification Symposium*, Volume 4, October, 1965.

11. ASME Power Test Codes, Supplement, Chapter 4, Part 5, *Flow Measurement, Instruments and Apparatus*, February 1959.

12. Bell, J.K., *Theoretical Investigation of the Flutter Characteristics of Supersonic Cascades with Subsonic Leading - Edge Locus*, Naval Post Graduate School Thesis, June, 1975.

13. Brix, C.W., Jr., *A Study of Supersonic Flow Past Vibrating Shells and Cascades*, Naval Post Graduate School Thesis, June, 1973.

14. Zierep, Jurgen, "Auftrieb und Widerstand Langerringflugel in Uberschallstromung", *Wissenschaftliche Gesellschaft fur Luftfahrt e. V.*, January 1957.

15. ARL report No. 74-0113,"*Development of a Time Dependent Nozzle*", Viets,H., July 1974.

16. Platzer, "Wind Tunnel Interference on Oscillating Airfoils in Low Supersonic Flow" *Acta Mechanica*, Vol. 16 , pages 115-126, 1973.

INITIAL DISTRIBUTION LIST

1.	Defence Documentation Center Cameron Station Alexandria, Virginia 22314	2
2.	Library, Code 0212 Naval Post Graduate School Monterey, California 93940	2
3.	Department Chairman, Code 57 Aeronautics Department Naval Post Graduate School Monterey, California 93940	1
4.	Professor M.F. Platzer, Code 57P Aeronautics Department Naval Post Graduate School Monterey, California 93940	5
5.	2/LT Donald L. Weiss 1115 Tedford Way Oklahoma City, Oklahoma 73116	1
6.	Dr. H. J. Mueller Research Administrator Code AIR-310 Naval Air Systems Command Washington, D.C. 20360	1

Thesis
W3823
c.1

165134

Weiss

An experimental investigation of the whistler nozzle and an analytical investigation of a ring wing in supersonic flow.

Thesis
W3823
c.1

165134

Weiss

An experimental investigation of the whistler nozzle and an analytical investigation of a ring wing in supersonic flow.

thesW3823
An experimental investigation of the whi
3 2768 001 95185 8
DUDLEY KNOX LIBRARY